iScience

CellPress
OPEN ACCESS

Article

EZH2 T367 phosphorylation activates p38 signaling through lysine methylation to promote breast cancer progression

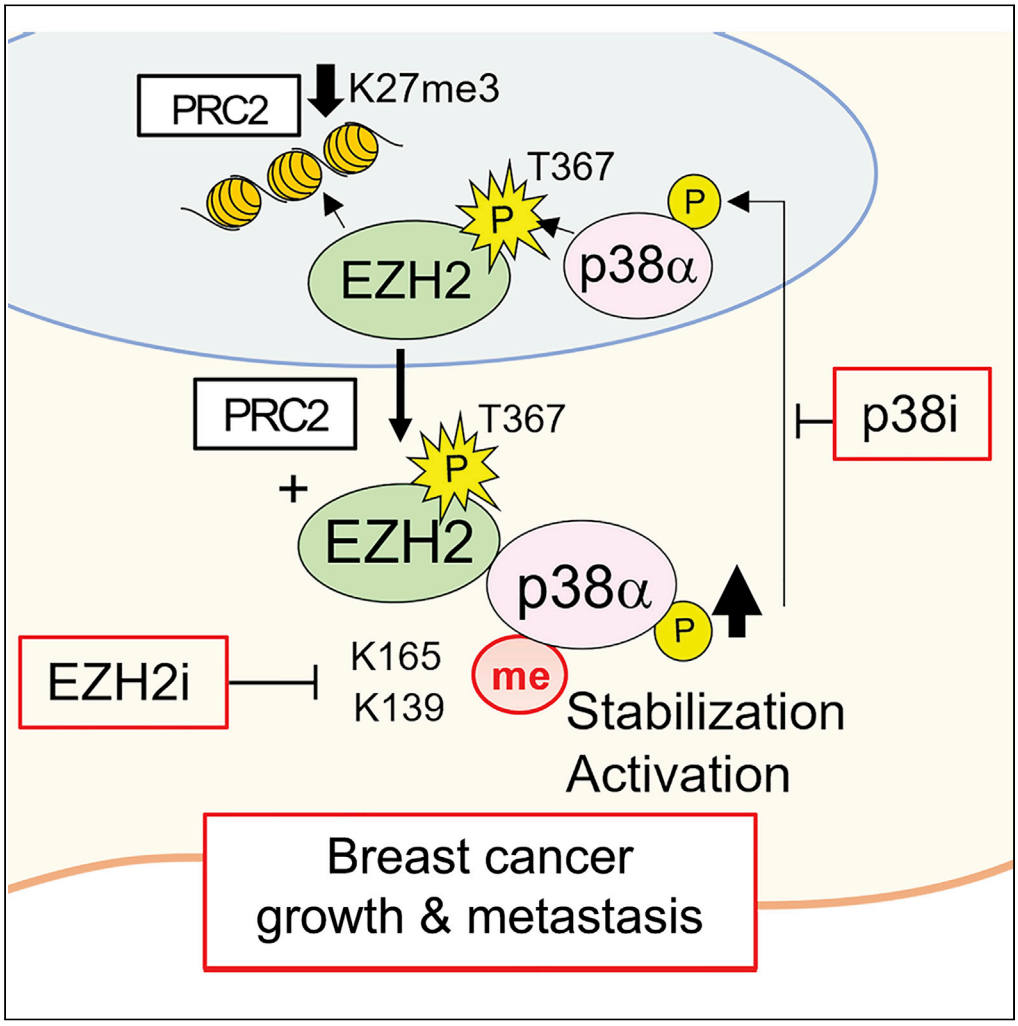

Maria E. Gonzalez, Giuseppina Daniela Naimo, Talha Anwar, ..., Euisik Yoon, Sebastiano Andò, Celina G. Kleer

kleer@umich.edu

Highlights

EZH2 methylates p38α protein at lysine 139 and lysine 165, increasing p38α stability

EZH2 phosphorylation at T367 is needed for cytosolic p38α methylation and activation

Dual inhibition of EZH2 and p38 enzymatic activities reduces breast cancer progression

Gonzalez et al., iScience *25*, 104827
August 19, 2022
https://doi.org/10.1016/j.isci.2022.104827

iScience

CellPress
OPEN ACCESS

Article

EZH2 T367 phosphorylation activates p38 signaling through lysine methylation to promote breast cancer progression

Maria E. Gonzalez,[1,2,9] Giuseppina Daniela Naimo,[1,3,9] Talha Anwar,[4] Alessandro Paolì,[1,3] Shilpa R. Tekula,[1,2] Suny Kim,[1] Natasha Medhora,[1] Shoshana A. Leflein,[1] Jacob Itkin,[1] Raymond Trievel,[5] Kelley M. Kidwell,[2,6] Yu-Chih Chen,[7] Loredana Mauro,[3] Euisik Yoon,[8] Sebastiano Andò,[3] and Celina G. Kleer[1,2,10,*]

SUMMARY

Triple-negative breast cancers (TNBCs) are frequently poorly differentiated with high propensity for metastasis. Enhancer of zeste homolog 2 (EZH2) is the lysine methyltransferase of polycomb repressive complex 2 that mediates transcriptional repression in normal cells and in cancer through H3K27me3. However, H3K27me3-independent non-canonical functions of EZH2 are incompletely understood. We reported that EZH2 phosphorylation at T367 by p38α induces TNBC metastasis in an H3K27me3-independent manner. Here, we show that cytosolic EZH2 methylates p38α at lysine 139 and 165 leading to enhanced p38α stability and that p38 methylation and activation require T367 phosphorylation of EZH2. Dual inhibition of EZH2 methyltransferase and p38 kinase activities downregulates pEZH2-T367, H3K27me3, and p-p38 pathways *in vivo* and reduces TNBC growth and metastasis. These data uncover a cooperation between EZH2 canonical and non-canonical mechanisms and suggest that inhibition of these pathways may be a potential therapeutic strategy.

INTRODUCTION

Breast cancer metastasis continues to be responsible for over 40,000 deaths in the U.S. (Siegel et al., 2018) Triple-negative breast cancer (TNBC) comprise 15–20% of invasive carcinomas but are responsible for a disproportionate number of deaths because of their high metastatic ability and limited effective therapeutic options (Vagia et al., 2020). Patients with metastatic TNBC have a median overall survival of 24 months and a 5-year survival rate of 12% (McGuire et al., 2017; Vagia et al., 2020).

A central feature of cancer cells is deregulated differentiation, a process by which neoplastic cells lose morphological characteristics of mature cells, acquire nuclear pleomorphism, and invade into the surrounding tissues. Dysregulation of genes governing cell type identity may lead to malignant transformation. The transcriptional memory of cells is tightly regulated through epigenetic mechanisms largely by polycomb and trithorax group proteins (Lee et al., 2006; Margueron and Reinberg, 2011; Richly et al., 2011; Sparmann and van Lohuizen, 2006). Enhancer of zeste homolog 2 (EZH2) is the catalytic subunit of polycomb repressive complex 2 (PRC2) and functions as a lysine methyl transferase, which mediates transcriptional silencing through trimethylation of histone H3 on lysine 27 (H3K27me3) (Cao and Zhang, 2004; Kuzmichev et al., 2004; Margueron and Reinberg, 2011; Richly et al., 2011; Shen et al., 2008; Sparmann and van Lohuizen, 2006).

In addition to a crucial function in normal cell fate and differentiation, EZH2 protein is upregulated in multiple human malignancies, where it functions as an oncogene (Kim et al., 2013; Kleer et al., 2003; Margueron and Reinberg, 2011; Richly et al., 2011; Sparmann and van Lohuizen, 2006; Varambally et al., 2002). In breast cancer, we have shown that EZH2 overexpression promotes breast cancer initiation, invasion, and metastasis (Ding et al., 2006; Gonzalez et al., 2009; Kleer et al., 2003). Using human breast tissue samples, we reported that EZH2 expression is low in normal epithelium and increases with the severity of atypia. EZH2 levels progressively increase in atypical ductal hyperplasia, ductal carcinoma *in situ*, and invasive carcinomas, with the highest expression in distant metastasis (Ding et al., 2006; Ding and Kleer, 2006; Kleer

[1]Department of Pathology, University of Michigan Medical School, Ann Arbor, MI 48109, USA

[2]Rogel Cancer Center, University of Michigan, Ann Arbor, MI, USA

[3]Department of Pharmacy, Health and Nutritional Sciences, University of Calabria, 87036 Rende (CS), Italy

[4]Department of Internal Medicine, Michigan Medicine, Ann Arbor, MI, USA

[5]Department of Biological Chemistry, University of Michigan, Ann Arbor, MI, USA

[6]Department of Biostatistics, School of Public Health, University of Michigan, Ann Arbor, MI, USA

[7]UPMC Hillman Cancer Center, Department of Computational and Systems Biology, Department of Bioengineering, University of Pittsburgh School of Medicine, Pittsburgh, PA 15232, USA

[8]Department of Electrical Engineering and Computer Science and Department of Biomedical Engineering, University of Michigan, Ann Arbor, MI, USA

[9]These authors contributed equally

[10]Lead contact

*Correspondence: kleer@umich.edu

https://doi.org/10.1016/j.isci.2022.104827

et al., 2003; Raaphorst et al., 2003). EZH2 overexpression in primary breast carcinomas is significantly associated with estrogen receptor (ER)–negative status, features of poor tumor differentiation, and is an independent biomarker of patient survival (Bachmann et al., 2006; Gonzalez et al., 2009; Kleer et al., 2003; Pang et al., 2012).

The oncogenic functions of EZH2 in breast cancer and other malignancies have been attributed to its transcriptional repression function through H3K27 trimethylation (Anwar et al., 2018; Cha et al., 2005; Gonzalez et al., 2014; Hoffmeyer et al., 2017; Kim et al., 2013; Morey and Helin, 2010; Simon and Kingston, 2009; Xu et al., 2012). Our laboratory has reported that p38α mitogen-activated kinase (encoded by the *MAPK14* gene), a major transducer of stress signals from the microenvironment and tumor promoter (Igea and Nebreda, 2015; Pereira et al., 2013; Wagner and Nebreda, 2009), binds to and phosphorylates EZH2 at threonine 367 to enhance TNBC metastasis in an H3K27me3-independent manner (Anwar et al., 2018). We have shown that pEZH2-T367 accumulates in the cytoplasm of TNBC cells where it interacts with vinculin and other cytoskeletal regulatory proteins (Anwar et al., 2018). Recent studies have shown that histone methyltransferases including EZH2 and SET7/9 can methylate non-histone proteins to activate their signaling pathways (Huang et al., 2006; Kim et al., 2013; Lu et al., 2010; Stark et al., 2011; Yang et al., 2010). EZH2 has been reported to methylate STAT3 protein and increase STAT3 activation in glioblastoma stem cells, in a mechanism that requires a specific EZH2 phosphorylation (Kim et al., 2013). However, the non-histone substrates of EZH2 and the detailed mechanism by which EZH2 regulates TNBC progression are currently unknown. In this study, we demonstrate that EZH2 methylates p38α *in vitro* and in TNBC mouse models, leading to enhanced p38 protein stability, which requires T367 phosphorylation of EZH2. We identify that EZH2 lysine methyltransferase and p38 kinase activities cooperate to promote breast cancer growth and metastasis and that the combined use of EZH2 and p38 inhibitors decreases cancer progression in mouse models of TNBC.

RESULTS

pEZH2-T367 upregulation is associated with increased p38 phosphorylation in patient-matched primary and metastatic breast carcinomas

We evaluated the expression of pEZH2-T367 using immunohistochemistry on 16 primary carcinomas and matched distant metastasis from the same patients. The clinicopathological features of this cohort and expression of p-p38 were previously reported (Moore et al., 2013). We observed that when present, pEZH2-T367 and p-p38 were expressed in the cytoplasm and in the nucleus of cancer cells (Figure 1A). pEZH2-T367 and p-p38 were scored as high when >10% of the cancer cells showed moderate or strong staining and were scored as low when staining was present in <10% of tumor cells based on our previous studies (Anwar et al., 2018; Gonzalez et al., 2011). We found that the expression of pEZH2-T367 and p-p38 are upregulated in the distant metastasis compared to the patient-matched primary tumors (χ^2 $p = 0.025$ and $p = 0.03$, respectively) (Figure 1B). Further, we identified a novel significant association between pEZH2-T367 and p-p38 protein expression in invasive and metastatic carcinomas of the breast. Of the primary carcinomas, pEZH2-T367 and p-p38 are concordantly expressed in 12 of 16 (75%) tumors, with both proteins being low in 56.25% and high in 18.75%. Of the metastatic breast carcinomas, pEZH2-T367 and p-p38 are concordantly expressed in 11 of 16 (68.75%), with both proteins being low in 12.5% and high in 56.75% of the tumors (χ^2 $p = 0.021$, Figure 1C).

EZH2 methylates p38α protein in TNBC, and EZH2 phosphorylation at threonine 367 enhances p38α methylation and phosphorylation

Based on our data that EZH2 directly binds to p38α (Anwar et al., 2018) and that EZH2 regulates p38 activity (Moore et al., 2013), we tested the hypothesis that EZH2 may methylate p38α to activate p38 signaling in TNBC and that T367 phosphorylation may regulate this function. Toward this, we employed MDA-MB-231 cells, patient-derived TNBC cells T4 (Gonzalez et al., 2014) and Vari068, and cells derived from MMTV-Cre;*Ccn6*$^{fl/fl}$ mouse TNBC metaplastic carcinomas (Djomehri et al., 2020; Martin et al., 2017). Reciprocal immunoprecipitation (IP) and Western blot experiments using anti-p38α and methylated lysine-specific antibodies showed that methylated p38α is present in lysates of all tumor cells and that EZH2 knockdown (KD) reduces methyl-p38α in all TNBC cell models tested (Figures 2A and S1A).

We next measured EZH2 lysine methyltransferase (KMTase) activity on p38α in whole-cell lysates of MDA-MB-231 cells. We targeted EZH2 genetically (shRNA-mediated KD) or pharmacologically with EPZ-6438, a

A

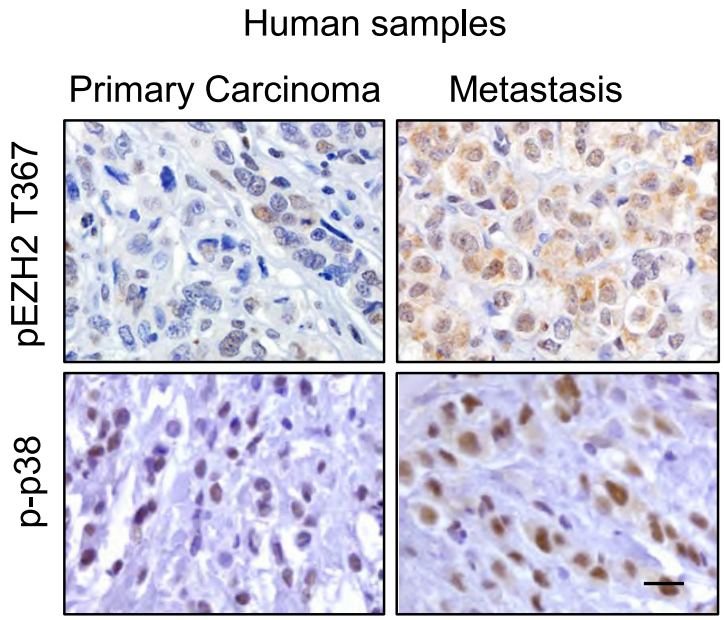

B

	pEZH2 T367 Low	pEZH2 T367 High	Total
Primary	9 (56.2%)	7 (43.8%)	16
Metastasis	2 (12.5%)	14 (87.5%)	16

Fisher exact test p=0.023

C

	pEZH2 ^{Low} / p-p38 ^{Low}	pEZH2 ^{High} / p-p38 ^{High}	Total
Primary	9 (56.25%)	3 (18.75%)	16
Metastasis	2 (12.5%)	9 (56.75%)	16

Fisher exact test p=0.012

Figure 1. pEZH2-T367 and p-p38 are significantly upregulated in human breast cancer metastasis compared to matched primary tumors from the same patient

(A) Representative images of matched primary human breast carcinomas and metastasis (n = 16 patients) immunostained for pEZH2-T367 and p-p38 (600x). pEZH2-T367 is upregulated in the cytoplasm of metastatic cells compared to the primary tumor. Bars 50 μm.

(B) Distribution of pEZH2-T367 protein expression in the 16 primary breast carcinomas and matched metastasis; the number of primary and metastatic breast carcinomas with low and high pEZH2-T367.

(C) Association between pEZH2-T367 and p-p38 expression in primary and metastatic carcinomas of the breast; 56.75% of metastasis exhibit high expression of both pEZH2-T367 and p-p38.

potent and selective lysine methyltransferase inhibitor (Knutson et al., 2014), and then assessed the methylation status of p38α in MDA-MB-231 cells using a bioluminescence-based KMTase assay and p38α protein as substrate. In both cases, p38α methylation was markedly decreased (Figure 2B lanes 1–3). Methylated p38α was rescued by ectopic WT-EZH2 and reduced by EPZ-6438 treatment (Figure 2B lanes 4–5). Extending the relevance of these data to human disease, treatment with EPZ-6438 was sufficient to reduce

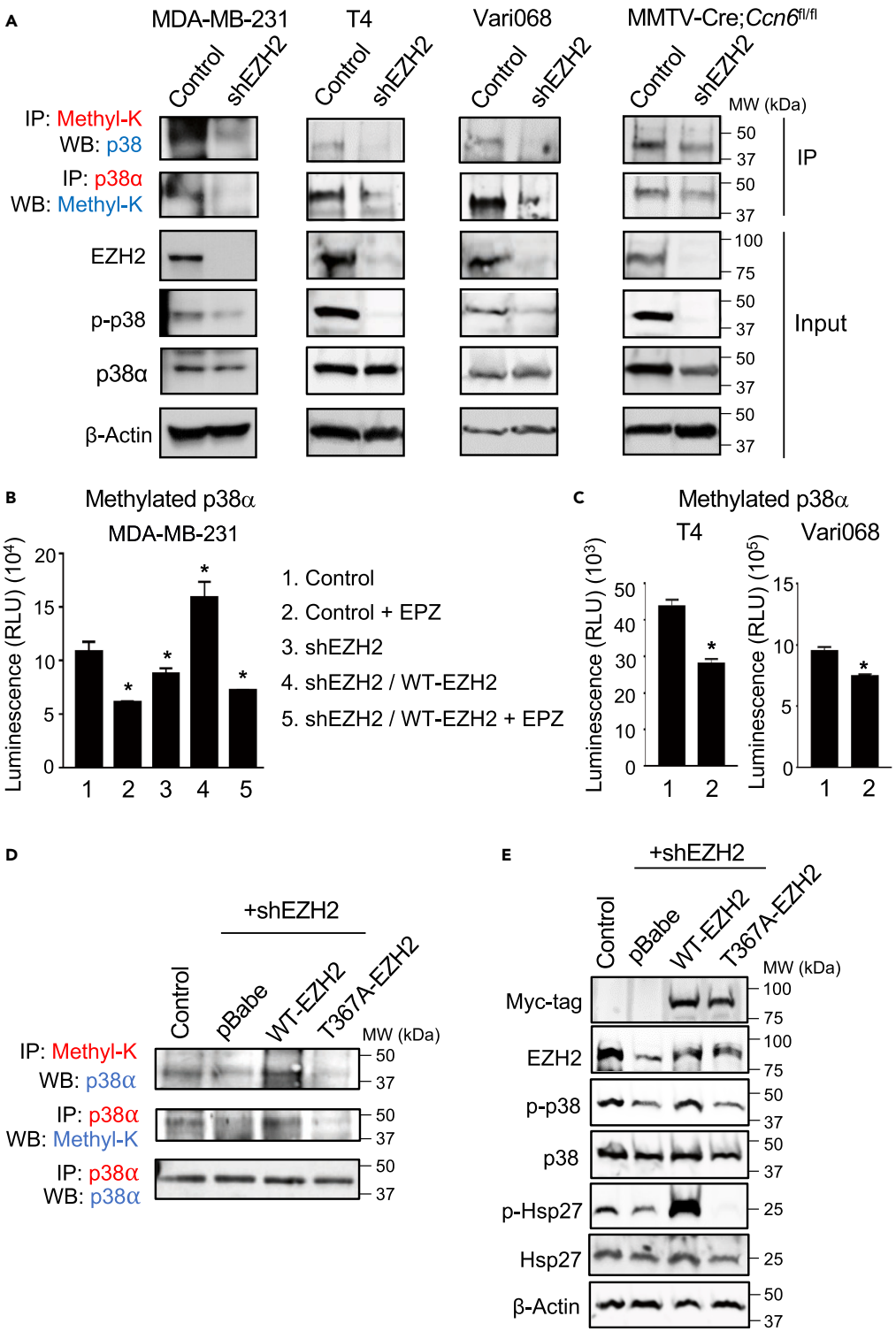

Figure 2. EZH2 methylates p38α, and EZH2 phosphorylation at T367 is critical for p38α methylation and phosphorylation in TNBC

(A) Co-immunoprecipitation (co-IP) and immunoblots of methylated p38α in a panel of breast cancer cells. EZH2 shRNA knockdown decreased methylated p38α.

(B) Lysine N-methyltransferase (KMTase) activity assay in whole-cell lysates of MDA-MB-231 cells at the indicated conditions. KMTase activity was assessed using 0.1 mg/mL of human recombinant p38α and measuring S-adenosyl

Figure 2. *Continued*
homocysteine (SAH) production detected by bioluminescence. shEZH2 and EPZ significantly reduced methylated p38α compared to control (lanes 1–3), which was rescued by WT-EZH2 (lane 4). EPZ reduced methylated p38α compared to WT-EZH2 (lanes 4–5). Bars depict mean ± SEM, *p ≤ 0.05.
(C) KMTase activity assay in whole-cell lysates of T4 and Vari068 patient-derived TNBC cells control and treated with EPZ as in (B). Bars show mean ± SEM, *p ≤ 0.05.
(D) IP and immunoblots of methylated p38α in MDA-MB-231 cells transduced with scrambled shRNA (control) or 3′ UTR EZH2-targeting shRNA (shEZH2) rescued with Myc-tagged WT-EZH2, T367A-EZH2, or vector (pBabe).
(E) Immunoblot of cells in (D).

methylated p38α in T4 and Vari068 patient-derived TNBC cells (Figure 2C). Similar results were obtained with shEZH2 KD (Figure S1B).

We investigated the role of T367 phosphorylation in EZH2-mediated p38α methylation and activation by reciprocal IP-WB. EZH2 KD reduced methyl-p38α and p-p38 compared to scrambled controls, which was rescued by WT-EZH2. In contrast, ectopic expression of T367A-EZH2 failed to rescue methyl-p38α and p-p38 (Figures 2D and 2E). Using proximity ligation assays with confocal microscopy, we found that endogenous pEZH2-T367 interacts with p38α (<40 nm apart) in the nucleus and cytoplasm of breast cancer cells (Figure S2A). In contrast to ectopic WT-EZH2, T367A-EZH2 reduced the cytoplasmic EZH2-p38α interaction without affecting the nuclear interaction between these proteins (Figure S2B). Cell fractionation experiments show that T367A-EZH2 reduced levels of p-p38 and methyl-p38α in the cytosolic fractions of MDA-MB-231 cells compared to WT-EZH2 (Figures S2C and S2D). Further supporting that pEZH2-T367 may methylate p38 in the cytoplasm, proximity ligation assay (PLA) studies show that endogenous pEZH2-T367 interacts with EED in the cytoplasm of MDA-MB-231 cells and that T367A-EZH2 inhibits this interaction (Figure S2E). Together, these results demonstrate that EZH2 methylates p38α and that EZH2 phosphorylation at T367 enhances p38α methylation and phosphorylation *in vivo* and *in vitro*. These data also suggest that T367 phosphorylation mediates EZH2-p38 cytoplasmic interaction and function.

EZH2 methylates p38α at lysine residues 139 and 165 to enhance p38α stability and function

To elucidate the specific sites of p38α methylation, we carried out liquid chromatography with tandem mass spectrometry (LC-MS-MS) analyses using recombinant GST-p38α and histone H3, each incubated with or without recombinant PRC2 complex (EZH2/EED/SUZ12/RbAp48/AEBP2) and S-adenosyl methionine methyl donor. LC-MS-MS indicated that PRC2-containing EZH2 induces p38α monomethylation at K139 and K165 and trimethylation at K139, which were confirmed by γ and β ion studies (Figures 3A and S3A).

Studies have shown that arginine methylation of p38α by Prmt7 (Jeong et al., 2020) and Prmt1 (Hua et al., 2013) increases p38α activation and promotes myoblast and erythroid differentiation, respectively, and that Prmt1-mediated p38α arginine methylation may facilitate protein stabilization (Hua et al., 2013; Liu et al., 2020). These data suggested the hypothesis that methylation by EZH2 may enhance p38α protein stability. We examined the protein stability of p38α by means of a pulse-chase assay with cycloheximide, an inhibitor of new protein biosynthesis. EZH2 shRNA downregulation or inhibition of EZH2 methyltransferase activity with GSK-343 significantly increased p38α turnover in MDA-MB-231 cells compared to controls (Figures 3B and 3C), suggesting that methylation enhances the stability of p38α protein.

To directly test the relevance of K139 and K165 methylation on p38α stability and function, we generated HA-tagged p38α mutants by replacing each lysine with Ala (K139A, K165A, and K139A/K165A). We overexpressed the p38α mutants in TNBC cells and performed co-IP experiments to assess their methylation status. While ectopic wild-type p38α was methylated, methylation was reduced in K139A, K165A, and K139A/K165A mutants (Figure 3D). Cycloheximide pulse-chase experiments revealed that K139A, K165A, and K139A/K165A had an increased turnover rate (half-life <9 h) compared to wild-type p38α (half-life >18 h) (Figure 3E). The proteasome inhibitor MG-132 increased the abundance of ubiquitin conjugates of p38α-mutant K139A/K165A compared to wild-type p38α, suggesting that the increased turnover is regulated by the ubiquitin-proteasome pathway (Figure 3F). Supporting that p38α methylation positively regulates p38 activity in TNBC cells, ectopic expression of HA-tagged p38α methylation site mutants had lower levels of p-p38 and its downstream phosphorylation target p-Hsp27 (Figure S3B). Activation of p38α occurs through a dual phosphorylation event at T180/T182 by upstream kinases MKK3 and MKK6 (Zarubin and Han, 2005). Transduction with an inducible, constitutively activated MKK6 mutant (MKK6EE)

A

Protein	Sequence Coverage	me	me2	me3
p38α	86%	K139, K165	none	K139
H3	66%	K27	K27	K27

B

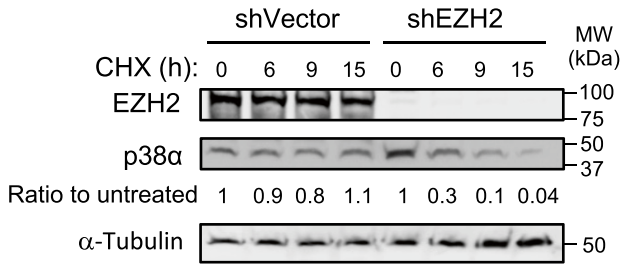

C

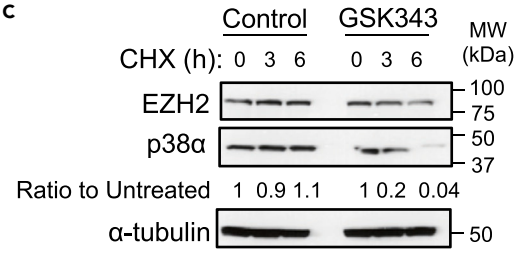

D

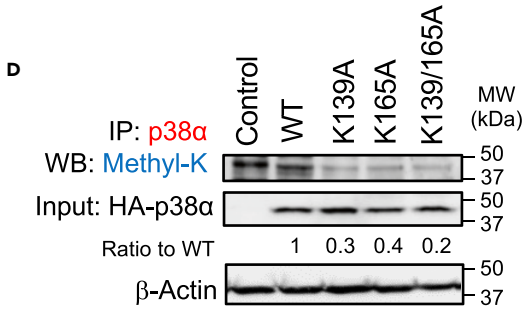

E

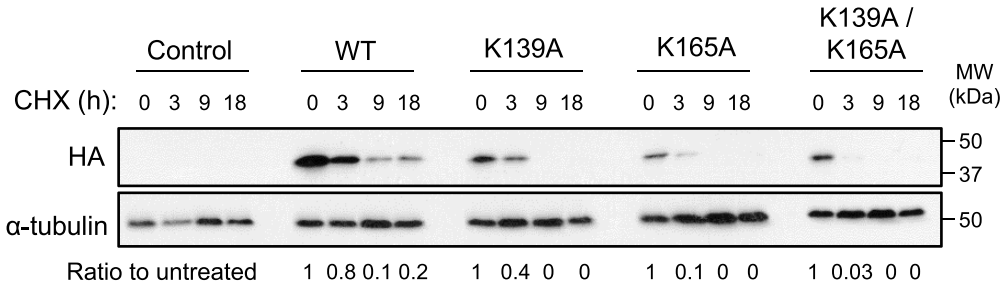

F

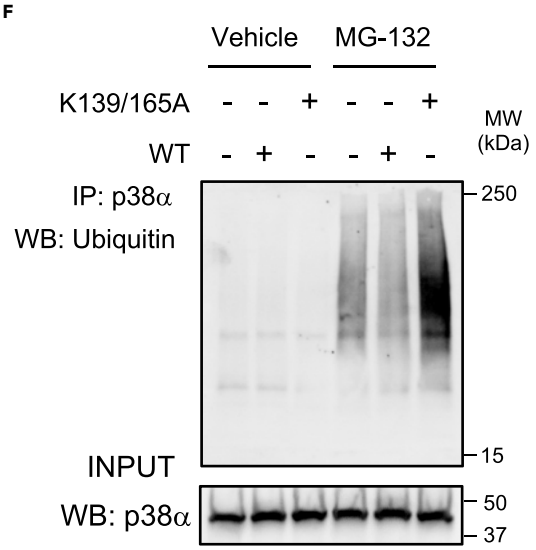

G

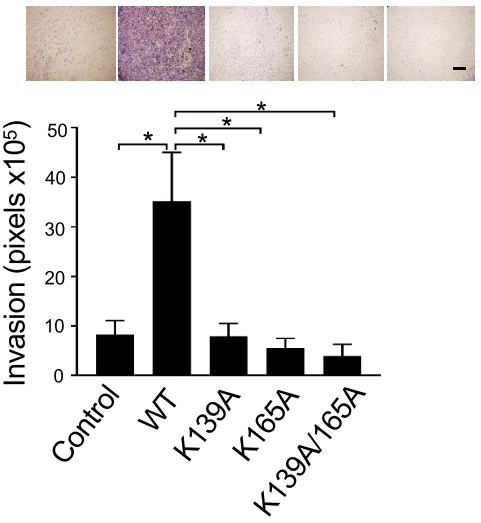

Figure 3. EZH2 methylates p38α protein at lysine 139 and lysine 165 leading to enhanced p38α protein stability

(A) Schematic representation of p38 protein indicating the position of its functional domains and methylation sites (red dots). The amino acid positions of each domain are indicated below the structures. The table summarizes the unique sites of methylation identified by LC-MS-MS analyses of methylated proteins. Recombinant histone H3 and GST-p38α were incubated with or without recombinant PRC2 complex (EZH2/EED/SUZ12/RbAp48/AEBP2) and S-adenosyl methionine methyl donor in sodium phosphate-buffered HMTase buffer solution for one hour at 37°C. Samples were subsequently run on a gel and digested in-gel using trypsin or Arg-C and analyzed for monomethylation, dimethylation, and trimethylation by LC-MS/MS. The presence of methylation was confirmed by β- and γ-ion.

(B) Pulse-chase analysis of MDA-MB-231 shVector and shEZH2 treated with 100 μg/mL of cycloheximide (CHX) at the indicated time points. Cell extracts were immunoblotted with anti-EZH2 and anti-p38α. α-Tubulin was used as the loading control.

(C) Pulse-chase analysis for MDA-MB-231 treated with vehicle (control) or GSK-343 (1 μM) for 48 h and treated with 100 μg/mL of cycloheximide (CHX) at the indicated time points. Cell extracts were immunoblotted with anti-EZH2 and anti-p38α. α-Tubulin was used as the loading control.

(D) HA-tagged p38α wild-type and p38α mutants K139A, K165A, and K139A/K165A were transduced into MDA-MB-231 cells and subjected to IP and WB using anti-p38α and anti-pan methyl-K antibody. Actin was used as the loading control.

(E) CHX pulse-chase assay of cells in (D).

(F) Ubiquitination assay. Indicated cells were treated with the proteasome inhibitor MG-132 (50 μM) for 5 h or vehicle. Whole-cell extracts were subsequently immunoprecipitated by anti-magnetics A beads followed by immunoblot using antibodies against ubiquitin and p38α.

(G) Invasion assay of MDA-MB-231 cells transduced with HA-tagged p38α wild-type and p38α mutants K139A, K165A, and K139A/K165A. Scale bar, 10 μm. Bars show mean ± SEM, *$p \leq 0.05$.

(Zarubin and Han, 2005) in 293T elevated the level of phosphorylated wild-type p38α relative to uninduced control; however, MKK6EE failed to increase phosphorylated K139A/K165A-p38α (Figure S3C). Consistent with reduced p38α activity, ectopic expression of p38α K139A, K165A, and K139A/K165A mutants failed to increase TNBC cell invasion and proliferation compared to wild-type p38α (Figures 3G and S3D). Collectively, these data show that EZH2 methylates p38α at lysine residues 139 and 165 leading to increased p38α protein stability and pro-invasion function in TNBC.

EZH2 methyltransferase and p38 kinase activities cooperate to promote breast cancer progression *in vivo* and *in vitro*

Given our identification of a reciprocal EZH2-p38α mechanism, we hypothesized that EZH2 and p38α may work in concert to promote neoplastic features in TNBC. To test this potentially important mechanistic and clinical hypothesis, we inhibited EZH2 lysine methyltransferase and p38 kinase activities with specific small-molecule inhibitors. To reduce EZH2 methyltransferase activity, we employed GSK-343 and EPZ-6438, and p38 kinase activity was inhibited using SB202190 (p38i), which were shown to reduce breast cancer tumorigenic functions *in vivo* (Gulati et al., 2018; Hoy, 2020; Italiano et al., 2018; Wu et al., 2014).

As expected, GSK-343 (and EPZ-6438) reduced H3K27me3 protein levels and signals on chromatin at gene promoters compared to controls (Figures 4A and S4A–S4C). Consistent with our previous study (Anwar et al., 2018), p38i reduced pEZH2-T367 protein levels and increased H3K27me3 protein levels and peaks at gene promoters compared to control (Figures 4A and S4A–S4D). Combined inhibition of EZH2 and p38 catalytic activities reduced pEZH2-T367 and H3K27me3 protein levels and signals on chromatin compared to p38i (Figures 4A, S4A, and S4C).

GSK-343 and SB202190 had 50% inhibitory concentrations (IC_{50}) of 4.08 μM and 28 μM, respectively. Combined treatment reduced MDA-MB-231 cell growth compared to each drug alone (Figure 4B) and showed strong synergistic effect in MDA-MB-231 and SUM149 cells (Figures 4C and S5A). Combination treatment of EZH2 and p38 inhibitors led to a stronger inhibition of cancer cell invasion and migration compared to single agents (Figures 4D, 4E, and S5B–S5D).

To determine the relevance of EZH2-p38α cooperation *in vivo*, we established NOD/SCID, nude, and syngeneic TNBC mouse models and subjected them to treatment with EPZ-6438, SB202190 (p38i), combination, or controls. Combined pharmacological inhibition of EZH2 and p38 activities significantly reduced primary tumor growth kinetics of orthotopic xenografts of MDA-MB-231 cells compared to single inhibitors and to the untreated control (Figures 5A and 5B). The effect on tumor growth was validated in a syngeneic basal-like 4T1 mouse model in BALB/c immune competent mice, where combined EPZ/p38i treatment significantly reduced tumor growth compared to single inhibitors and controls (Figures S6A and S6B). In heart inoculation studies in nude mice, combined EPZ/p38i treatment reduced MDA-MB-231 distant metastasis compared to the single inhibitors and to controls (Figures 5C and 5D).

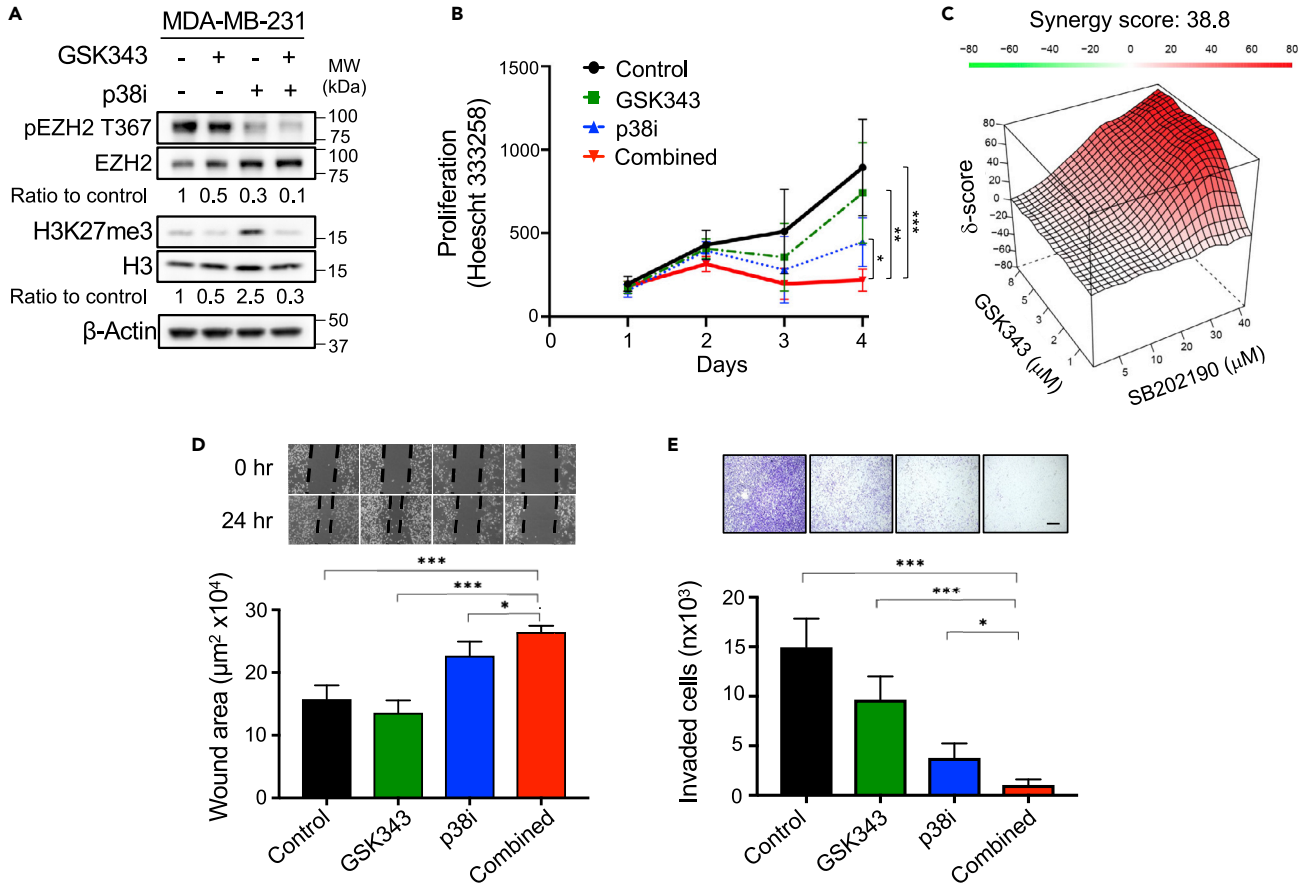

Figure 4. Combined pharmacological blockade of EZH2 and p38 enzymatic activities reduces neoplastic functions

(A) Immunoblots of MDA-MB-231 cells treated with GSK-343 (3 μM for 48 h), SB202190 (p38i, 20 μM for 48 h), or the combination.

(B) Cells in A were subjected to growth assays.

(C) Synergistic effect of EZH2 inhibitor and p38 inhibitor in MDA-MB-231 cells incubated with various doses of GSK-343 and SB202190 for 4 d. A matrix for synergy score was calculated (Ianevski et al., 2017).

(D and E) Wound healing assay to quantify cell migration (D) and reconstituted Boyden basement membrane-invasive chamber assay of MDA-MB-231 cells treated as in (A). Representative chambers after crystal violet staining are shown above bars. Data for B-E are from at least three independent experiments carried out in at least triplicate. Data for B, (D and E) are presented as mean ± SEM. *p ≤ 0.05; **p ≤ 0.01; ***p ≤ 0.005; ****p ≤ 0.0001.

Based on our data that EZH2 methylates p38α *in vitro* and that T367 phosphorylation is important for p38 methylation and activation, we sought to assess p38α methylation status in TNBC tumors and the effect of combined EPZ/p38i treatment on p38α methylation and activation *in vivo*. Primary MDA-MB-231 and 4T1 tumors were dissected and processed for Western blot and co-IP experiments. Methylated p38α was present in lysates from both models (Figures 5E and S6C). EPZ reduced p38α methylation in the tumors compared to controls. Combined EPZ/p38i treatment showed the lowest p38α methylation levels (Figure 5E). Consistently, in addition to reducing H3K27me3, combined EPZ/p38i treatment reduced pEZH2-T367 as well as p-p38 and its direct phosphorylation target p-Hsp27, demonstrating a downregulation of EZH2 non-canonical pathway compared to each inhibitor in isolation (Figure 5F). Histologically, combined EPZ/p38i was sufficient to promote gland formation and upregulation of the luminal cytokeratin-18 and reduced expression of basal cytokeratin-14 compared to the poorly differentiated control tumors with a basal phenotype (Figures S6D–S6F). Taken together, these data uncover a synergistic interaction between EZH2 and p38 enzymatic activities on TNBC growth and metastasis.

Pharmacological inhibition of EZH2 and p38 activities modifies gene expression in TNBC

To elucidate the molecular targets of the combined inhibition of EZH2-p38 enzymatic activities in TNBC, we performed RNA sequencing analyses of the primary MDA-MB-231 orthotopic xenografts treated with EPZ, p38i, combination, or control. Principal component analysis (PCA) of the tumor samples showed a

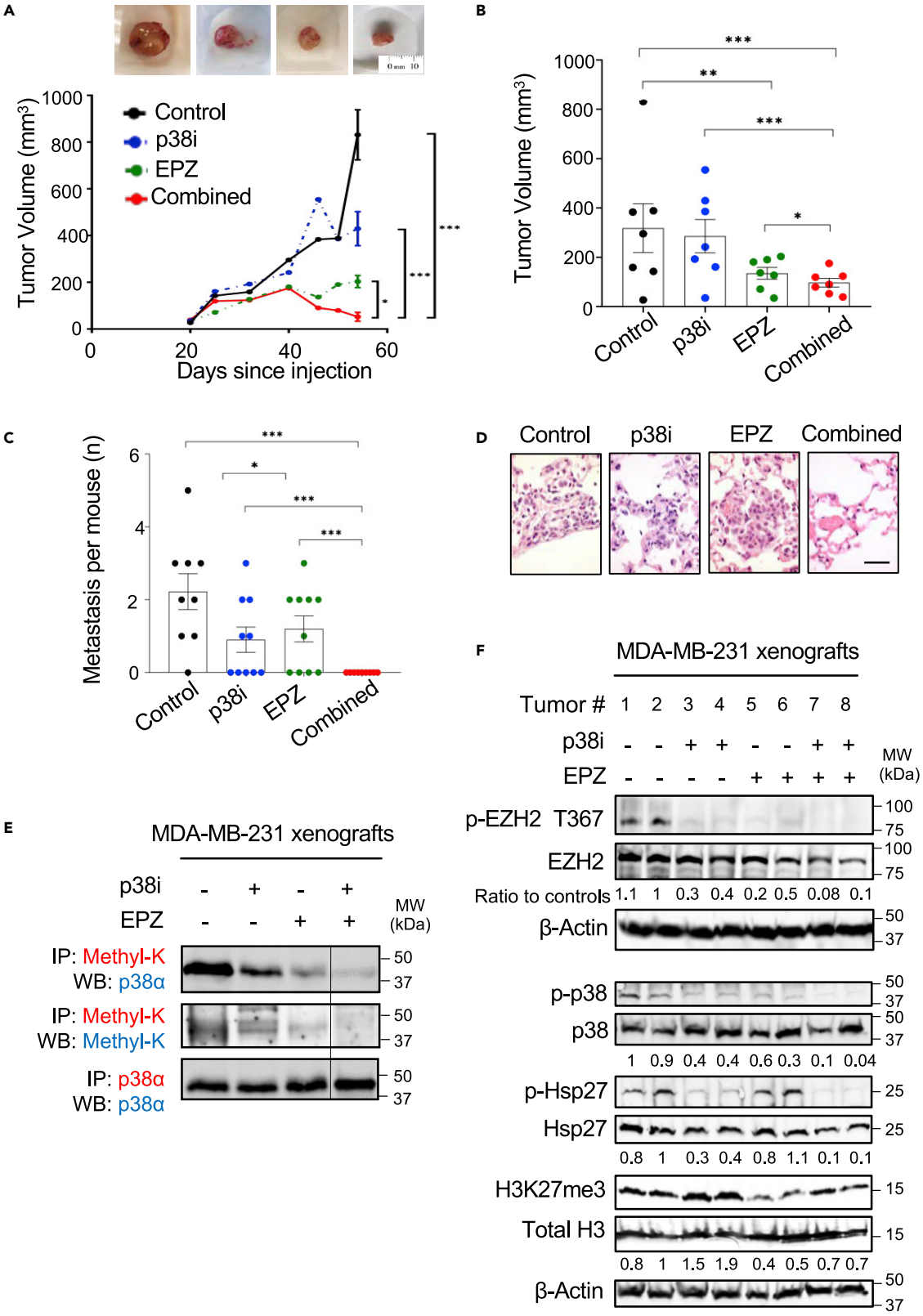
A
Tumor Volume (mm3)
Control
p38i
EPZ
Combined
Days since injection
B
Tumor Volume (mm3)
Control
p38i
EPZ
Combined
C
Metastasis per mouse (n)
Control
p38i
EPZ
Combined
D
Control
p38i
EPZ
Combined
E
MDA-MB-231 xenografts
p38i
EPZ
MW (kDa)
IP: Methyl-K
WB: p38α
IP: Methyl-K
WB: Methyl-K
IP: p38α
WB: p38α
F
MDA-MB-231 xenografts
Tumor # 1 2 3 4 5 6 7 8
p38i
EPZ
MW (kDa)
p-EZH2 T367
EZH2
Ratio to controls 1.1 1 0.3 0.4 0.2 0.5 0.08 0.1
β-Actin
p-p38
p38
1 0.9 0.4 0.4 0.6 0.3 0.1 0.04
p-Hsp27
Hsp27
0.8 1 0.3 0.4 0.8 1.1 0.1 0.1
H3K27me3
Total H3
0.8 1 1.5 1.9 0.4 0.5 0.7 0.7
β-Actin

Figure 5. Combined targeting of EZH2 and p38 enzymatic activities reduces primary breast cancer growth and metastasis

(A) Primary tumor growth curves of NOD/SCID mice orthotopically implanted with MDA-MB-231 cells. When primary tumors reached 100 mm^3, mice were treated intraperitoneally with EPZ-6438 (10 mg/kg/day), SB202190 (p38i, 1 mg/kg/day), combination, or control (4% DMSO-30% PEG 300-5% Tween 80), 5 days/week for 56 days (n = 10/group). Primary tumor growth as assessed by caliper measurements, shown as mean ± SEM.

(B) Quantification of tumor volume at day 56 shown as mean ± SEM.

(C) MDA-MB-231 cells were injected intracardially in nude mice (n = 10/group) and treated as in (A), for 3 weeks. Bars show the number of metastases per mouse in each group on day 21 after heart inoculation ±SEM.

(D) Representative H&E-stained sections of lung metastases. Magnification 600x. Scale bar 50 μm.

(E) Co-immunoprecipitation and immunoblots of methylated p38α in whole-cell lysates of primary MDA-MB-231 xenograft tumors derived from (A).

(F) Immunoblots for the indicated proteins in lysates obtained from the MDA-MB-231 primary orthotopic xenografts in (A). For A-C, *p ≤ 0.05; **p ≤ 0.01; ***p ≤ 0.005; ****p ≤ 0.0001.

distinction between control tumors compared to tumors treated with EPZ, p38i, or the combination (Figure S7A). Our studies identified the phosphoinositide 3-kinase (PI3K)–AKT pathway as one of the top pathways targeted by the combined EZH2-p38 enzymatic activities compared to controls (Figure 6A). Because EPZ/p38i treatment exerted the most robust effect on reducing TNBC growth and metastasis *in vivo* compared to EPZ and to p38i as single treatments, we interrogated pathways deregulated by EPZ/p38i treatment compared to single treatments. PI3K/AKT was the most significantly deregulated of the 13 pathways unique to EPZ/p38i treatment (Figures S7B and S7C). Validating the RNAseq data, EPZ/p38i treatment of MDA-MB-231 and 4T1 xenografts reduced pAKT protein levels compared to single inhibitors (Figures 6B and S8A). The translational potential of these findings is supported by data in clinical samples showing that PI3K/AKT signaling is active in over 50% of human breast cancer and in up to 25% of TNBC tumors (Baselga, 2011; Pascual and Turner, 2019).

Our laboratory has reported that EZH2 expression is significantly associated with pAKT1 in human breast cancer tissues and that EZH2 KD in TNBC cells reduces pAKT1 (Gonzalez et al., 2011). We observed that EZH2 KD reduced pAKT protein in patient-derived TNBC cells T4 and Vari068 and in MMTV-Cre;*Ccnδ*$^{fl/fl}$ TNBC cells (Figure S8B). We next investigated the mechanistic contribution of pEZH2-T367 and p38α methylation to pAKT levels. Ectopic expression of p38α mutants K139A, K165A, or K138A/K165A led to reduced pAKT levels compared to WT-p38α in MDA-MB-231 cells (Figure 6C). T367A-EZH2 was unable to rescue pAKT1 compared to WT-EZH2 (Figure 6D), suggesting that AKT activation depends at least in part on EZH2 T367 phosphorylation and p38α methylation. These data also demonstrate a role for the reciprocal EZH2-p38 cooperation in the activation of AKT in TNBC.

To assess the relevance of our studies to human breast cancer, we investigated the expression of pEZH2-T367 and pAKT proteins in 94 primary invasive carcinoma tissue samples arrayed in a tissue microarray by our laboratory (Kleer et al., 2003). Immunohistochemical analysis showed that when present, pEZH2-T367 protein was predominantly cytoplasmic and that pAKT protein was localized to the nuclei and the cytoplasm of breast cancer cells (Figure 6E) (Anwar et al., 2018; Gonzalez et al., 2011; McMullen et al., 2021). Cytoplasmic pEZH2-T367 and pAKT were scored as high when >10% of the cancer cells showed moderate or strong staining and were scored as low when staining was present in <10% of tumor cells (Anwar et al., 2018; Gonzalez et al., 2011; McMullen et al., 2021). We found a novel significant association between pEZH2-T367 and pAKT protein expression. Of the 94 tumors, 66 (70.2%) exhibited concordant expression of pEZH2-T367 and pAKT proteins (40.4% had high pEZH2-T367 and pAKT, and 29.8% had low pEZH2-T367 and pAKT; χ^2 P = 0.0001, Figure 6E). Collectively, this work supports a model where in addition to H3K27me3-mediated functions, EZH2 enhances breast cancer progression through p38α methylation and pathway activation, in a mechanism that requires a specific EZH2 phosphorylation at T367 (Figure 6F).

DISCUSSION

EZH2 has tumor-promoting functions in solid tumors including breast (Bachmann et al., 2006; Chang et al., 2011; Kleer et al., 2003; Moore et al., 2013; Pang et al., 2012), prostate (Cao et al., 2008; Varambally et al., 2002; Xu et al., 2012), liver (Sudo et al., 2005), melanoma (Bachmann et al., 2006; McHugh et al., 2007), as well as in hematological malignancies such as lymphoma and leukemia (Fiskus et al., 2006; Kim and Roberts, 2016; Raaphorst et al., 2000; Visser et al., 2001). The mechanism by which EZH2 contributes to cancer development and progression has been attributed mainly to H3K27me3-mediated transcriptional silencing, with non-canonical EZH2 functions still far from understood (Anwar et al., 2018; Cha et al., 2005; Gonzalez et al., 2014; Hoffmeyer et al., 2017; Kim et al., 2013; Morey and Helin, 2010; Simon and Kingston, 2009; Xu et al., 2012). In this study, we discover that EZH2 methylates p38α leading to enhanced p38

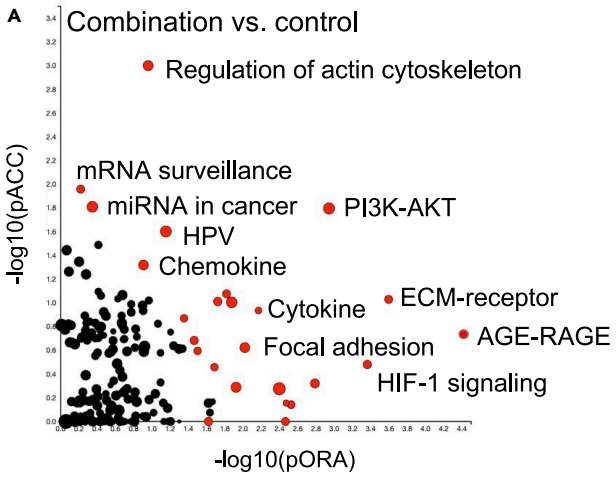

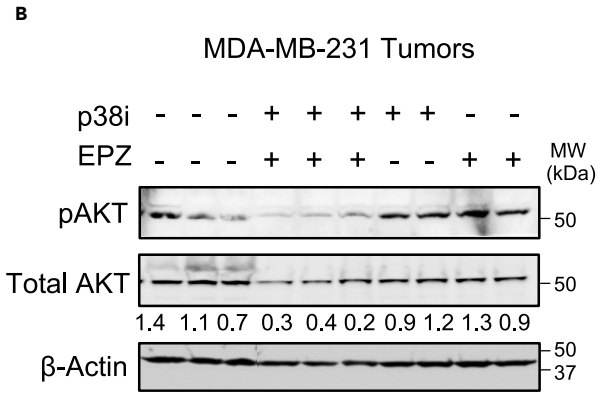

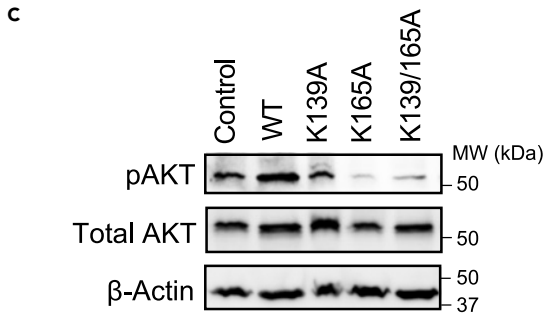

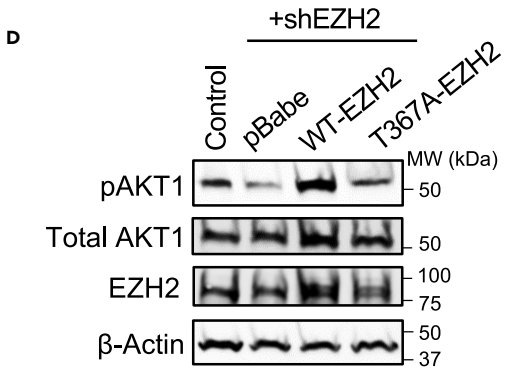

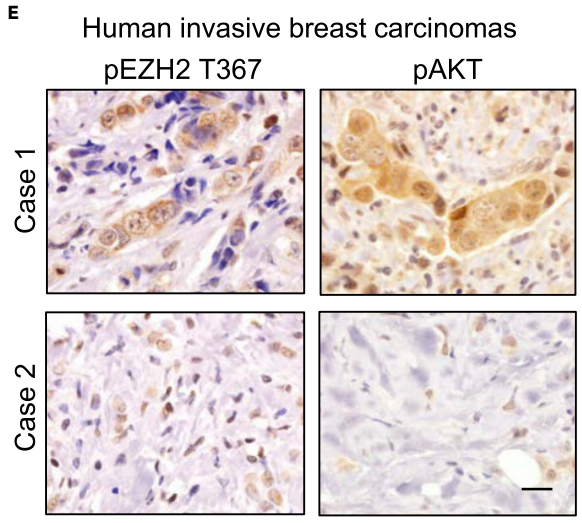

	pAKT Low	pAKT High
pEZH2 T367 Low	28 (29.8%)	12 (12.8%)
pEZH2 T367 High	16 (17%)	38 (40.4%)

Chi Square p=0.00024

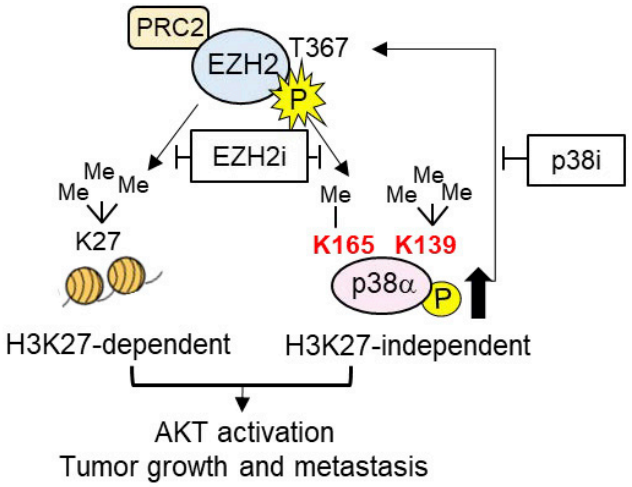

Figure 6. Combined inhibition of EZH2 methyltransferase and p38 kinase activities reduce AKT signaling *in vivo*

(A) RNA sequencing studies of mammary tumors treated with EPZ-6438 (10 mg/kg/day), SB202190 (p38i, 1 mg/kg/day), combination, or control (4% DMSO-30% PEG 300-5% Tween 80) and excised at day 56. The graph shows significantly deregulated pathways by the combination EPZ/p38i vs. control.

(B) Immunoblot of primary xenografts treated as indicated in (A). Combined EPZ/p38i reduces *p*-AKT compared to single inhibitors.

(C) Immunoblots for pAKT and total AKT in MDA-MB-231 cells transduced with HA-tagged WT-p38α, K139A-p38α, K165A-p38α, and K139A/K165A-p38α. P38α mutants display reduced pAKT levels compared to WT-p38α.

(D) Immunoblots of MDA-MB-231 EZH2 KD rescued with Myc-tagged WT-EZH2, T367A-EZH2, or vector (pBabe) show that T367 phosphorylation is necessary to upregulate pAKT1 without changes in total AKT1.

(E) Representative images of human primary invasive carcinomas. Case 1 shows an invasive high-grade ductal carcinoma with concordant high cyto-pEZH2-T367 and high pAKT, while case 2 shows an intermediate-grade invasive carcinoma with low expression of both proteins. Bars, 50 μm.

(F) Schematic illustrating our working model of EZH2 function in breast cancer through H3K27me3-dependent and independent activities. P and Me represent phosphorylation and methylation, respectively.

protein stability in breast cancer and reveal a novel cooperative mechanism between EZH2 and p38 that enhances breast cancer progression.

A main finding in the present study is that EZH2 directly methylates p38α protein at K139 and K165 to increase p38α stability and is critical for p38 function *in vitro* and *in vivo*. Although the precise molecular events that link p38α methylation to p38α activation need further investigation, our data show that they involve increased p38 protein stability via regulation of the ubiquitin-proteasome pathway. K139 is a MAPK-specific residue that tethers the C-tail to the αE-helix in the kinase domain of p38α and may play a role in protein activation, and K165 is located in the protein kinase domain of p38α (Nguyen et al., 2015). While lysine methylation of p38α was heretofore unknown, arginine methylation of p38α protein was shown to enhance its activity. The arginine methyltransferase PRMT1 was reported to methylate p38α at R49/R149, leading to p38 activation in erythroid precursors (Liu et al., 2020), and PRMT7 was found to methylate p38 at R70, also increasing its activation in myoblasts (Jeong et al., 2020). Together, these data identify EZH2 as a novel regulator of p38 in breast cancer through direct lysine methylation.

We have recently reported a direct and strong interaction between EZH2 and p38α in TNBC cells and showed that p38α phosphorylates EZH2 at T367 to increase breast cancer progression (Anwar et al., 2018). We found that pEZH2-T367 functions through H3K27me3-independent mechanisms, which involve EZH2 accumulation in the cytoplasm and binding to non-histone proteins (Anwar et al., 2018). A major finding in the present study is that EZH2 phosphorylation at T367 enhances p38α methylation and protein stability in TNBC cells, suggesting that EZH2 T367 phosphorylation may switch EZH2 activity toward H3K27me3-independent functions. Based on our work, this effect may be a consequence of pT367-induced EZH2 cytoplasmic localization and interaction with PRC2 members in the cytoplasm, facilitating methylation of non-histone proteins including p38α. Understanding the molecular basis of the regulation of EZH2 affinity for histone and non-histone substrates is of major interest in healthy and diseased cells and warrants further investigation.

The data presented herein have important biological and clinical implications for TNBC, an aggressive subtype of breast cancer with limited therapeutic options. Our results demonstrate that combined inhibition of EZH2 and p38 pathways has a profound effect on TNBC growth and dissemination compared to inhibition of each individual pathway. While dual EZH2 and p38 inhibition has not been explored until now, our current data are consistent with those of studies in breast cancer models demonstrating that EPZ-6438 reduced tumor volume of 4T1 cells and SUM149 cells compared to controls (Nie et al., 2019) and that another EZH2 methyltransferase inhibitor, GSK-126, reduced lung metastasis in patient-derived xenografts of TNBC (Yomtoubian et al., 2020). Also consistent with our data, p38 kinase inhibitors reduced metastasis in mouse models of breast cancer (Wu et al., 2014) and melanoma (Gui et al., 2020). In the clinic, an oral EZH2 inhibitor has been approved for the treatment of epithelioid sarcoma and has shown promising results in patients with diffuse large B-cell lymphoma (DLBCL) and other advanced tumors (Gounder et al., 2020; Sarkozy et al., 2020). In addition, there are at least five additional EZH2 inhibitors under evaluation in clinical trials (Dockerill et al., 2021). An oral p38 inhibitor was found beneficial in a phase I trial for aromatase refractory breast cancer in the metastatic setting (Patnaik et al., 2016). Future clinical studies are required to determine the potential of EZH2 and p38 activity inhibitor agents or their downstream targets for treatment of metastatic breast cancer and, possibly, other highly metastatic cancers that overexpress EZH2 and p38 proteins.

Using cell lines, cancer cells derived from patients, and animal models, we found that in addition to reducing H3K27me3, combined inhibition of EZH2 methyltransferase and p38 kinase activities maximally reduced EZH2 non-canonical pathway markers pEZH2-T367, methyl-p38, p-p38, and p-Hsp27 compared to single-inhibitor treatments *in vivo*. Studies from our laboratory and others have demonstrated that EZH2 signaling is an important regulator of mesenchymal-like phenotypes in breast cancer (Moore et al., 2013; Nie et al., 2020). Our current data show that combined EPZ/p38i treatment is sufficient to change a basal-like breast cancer phenotype toward improved glandular epithelial differentiation with increased expression of luminal cytokeratins. This suggests that combined inhibition of EZH2 and p38 may be a promising approach to improve tumor differentiation and reduce metastatic progression in a clinical setting.

Our unbiased RNA sequencing studies highlight the PI3K/AKT pathway as a specific target of the mechanistic cooperation between EZH2 and p38 in TNBC. Studies have shown that PI3K/AKT signaling is hyperactive in various human cancers including breast and that it is an important therapeutic target in this disease (Nie et al., 2020). RNA sequencing studies of treated tumors showed that PI3K/AKT pathway inhibition is a consequence of dual EPZ/p38i treatment compared to control and to each individual inhibitor. We demonstrate that both events, T367 phosphorylation of EZH2 and p38 methylation, play a role in AKT activation. Future studies aimed at understanding how H3K27me3 and pEZH2-T367 cooperate on the activation of AKT are warranted. Our studies in clinical samples of breast cancer showed a significant association between expression of pEZH2-T367 and pAKT in 40% of invasive carcinomas. These data suggest the hypothesis that detection of pEZH2-T367 and pAKT in primary breast cancer may be useful as a predictive biomarker of response to combined inhibition of EZH2 and p38 pathways in TNBC.

In conclusion, our results unveil a reciprocal mechanistic cooperation between EZH2 and p38α which enhances TNBC growth and metastasis. EZH2 methylates p38α, thereby enhancing p38α protein stability and activity in TNBC. EZH2-mediated methylation of p38α is positively regulated by T367 phosphorylation and is critical for the EZH2-p38 cooperation. Of special relevance to cancer biology, our data demonstrate that in aggressive breast cancer phenotypes, EZH2 functions through methylation of p38α in addition to H3K27me3 transcriptional silencing mechanisms. These data support the use of EZH2 and p38 activity inhibitors to effectively target the dual role of EZH2 in TNBC growth and metastasis.

Limitations of the study

In this study, we have shown that T367 phosphorylation of EZH2 plays a role in lysine methylation of p38α (MAPK14) protein. A limitation of the study is that anti-methyl-p38α recognizing the specific methylation sites is not available. Therefore, the frequency of this methylation event and association with p-p38 activation and pEZH2-T367 expression in human tissue samples of breast cancer has not been explored yet. While we show that p38i increases H3K27me3 protein and binding to gene promoters in TBNC cells, further work is needed to understand the consequences of this and of the combined treatment with EPZ on specific gene promoters. In addition, more work is needed to understand the mechanisms by which p38α methylation enhances p38α phosphorylation in cancer.

STAR★METHODS

Detailed methods are provided in the online version of this paper and include the following:

- KEY RESOURCES TABLE
- RESOURCE AVAILABILITY
  - Lead contact
  - Materials availability
  - Data and code availability
- EXPERIMENTAL MODEL AND SUBJECT DETAILS
  - Tissue samples and immunohistochemistry
  - Animal studies
- METHOD DETAILS
  - Cell culture and transductions
  - Western blot, immunoprecipitation, and protein stability assay
  - Lysine methyltransferase assay
  - LC-MS/MS analyses of methylated proteins

- Inhibitors and synergy score calculation
- Wound healing, invasion, migration, proliferation, and apoptosis assays
- Proximity ligation assays
- RNA sequencing and ChIP-sequencing studies

● QUANTIFICATION AND STATISTICAL ANALYSIS

SUPPLEMENTAL INFORMATION

Supplemental information can be found online at https://doi.org/10.1016/j.isci.2022.104827.

ACKNOWLEDGMENTS

We are grateful to members of the Kleer Laboratory for helpful discussion during this project. We thank Dr. Sofia Merajver for providing VARI-068 cells. This work was supported by National Institutes of Health grants R01CA125577 and R01CA107469 (C.G.K.), F30CA19084 (T.A.), Department of Defense Breast Cancer Research Program grant W81XWH-19-1-0093 (C.G.K), and University of Michigan Rogel Cancer Center support grant P30CA046592. C.G.K. is a Rogel Scholar. G.D.N. was supported by Italian Minister of University and Research (MIUR, D.D. n. 407/2018)-PON R&I 2014–2020, AIM "Attraction and International Mobility", A.P. was supported by MIUR Excellence Department Project funds (L.232/2016), awarded to the Department of Pharmacy, Health and Nutritional Sciences, University of Calabria, Italy.

AUTHOR CONTRIBUTIONS

M.E.G., T.A., G.D.N., and C.G.K. contributed to the design of the study, performed experiments, analyzed and interpreted data, and wrote the manuscript. G.D.N. and S.A. conceptualized and performed KMTase assays, S.A.L. and A.P. designed and performed immunoprecipitation/Western blot experiments, S.R.T. and M.E.G. performed *in vivo* experiments and drug treatments, S.A.L. and J.I. assisted with cell biology studies, K.M.K. performed statistical analyses of human tissues samples, Y-.C.C. and E.Y. performed the microfluidics migration assay, R.T. provided expertise on the KMT assays, S.A. and L.M. contributed to the writing, and C.G.K. conceived the study, contributed to the experimental design and human tissue analyses, and wrote the paper.

DECLARATION OF INTERESTS

E.Y, and Y-.C.C. filed a patent application on the microfluidic technology (Application No.:62/449,867 and PCT/US2018/014353). Other authors declare no competing interests.

Received: September 13, 2021
Revised: March 10, 2022
Accepted: July 20, 2022
Published: August 19, 2022

REFERENCES

Anwar, T., Arellano-Garcia, C., Ropa, J., Chen, Y.C., Kim, H.S., Yoon, E., Grigsby, S., Basrur, V., Nesvizhskii, A.I., Muntean, A., et al. (2018). p38-mediated phosphorylation at T367 induces EZH2 cytoplasmic localization to promote breast cancer metastasis. Nat. Commun. *9*, 2801. https://doi.org/10.1038/s41467-018-05078-8.

Bachmann, I.M., Halvorsen, O.J., Collett, K., Stefansson, I.M., Straume, O., Haukaas, S.A., Salvesen, H.B., Otte, A.P., and Akslen, L.A. (2006). EZH2 expression is associated with high proliferation rate and aggressive tumor subgroups in cutaneous melanoma and cancers of the endometrium, prostate, and breast. J. Clin. Oncol. *24*, 268–273.

Baselga, J. (2011). Targeting the phosphoinositide-3 (PI3) kinase pathway in breast cancer. Oncologist *16* (*Suppl 1*), 12–19. https://doi.org/10.1634/theoncologist.2011-S1-12.

Cao, Q., Yu, J., Dhanasekaran, S.M., Kim, J.H., Mani, R.S., Tomlins, S.A., Mehra, R., Laxman, B., Cao, X., Yu, J., et al. (2008). Repression of E-cadherin by the polycomb group protein EZH2 in cancer. Oncogene *27*, 7274–7284. https://doi.org/10.1038/onc.2008.333onc2008333.

Cao, R., and Zhang, Y. (2004). The functions of E(Z)/EZH2-mediated methylation of lysine 27 in histone H3. Curr. Opin. Genet. Dev. *14*, 155–164.

Cha, T.L., Zhou, B.P., Xia, W., Wu, Y., Yang, C.C., Chen, C.T., Ping, B., Otte, A.P., and Hung, M.C. (2005). Akt-mediated phosphorylation of EZH2 suppresses methylation of lysine 27 in histone H3. Science *310*, 306–310.

Chang, C.J., Yang, J.Y., Xia, W., Chen, C.T., Xie, X., Chao, C.H., Woodward, W.A., Hsu, J.M., Hortobagyi, G.N., and Hung, M.C. (2011). EZH2 promotes expansion of breast tumor initiating cells through activation of RAF1-beta-catenin signaling. Cancer Cell *19*, 86–100. https://doi.org/10.1016/j.ccr.2010.10.035.

Chen, Y.C., Allen, S.G., Ingram, P.N., Buckanovich, R., Merajver, S.D., and Yoon, E. (2015). Single-cell migration chip for chemotaxis-based microfluidic selection of heterogeneous cell populations. Sci. Rep. *5*, 9980. https://doi.org/10.1038/srep09980srep09980.

Chen, Y.-C., Gonzalez, M.E., Burman, B., Zhao, X., Anwar, T., Tran, M., Medhora, N., Hiziroglu, A.B., Lee, W., Cheng, Y.H., et al. (2019). Mesenchymal stem/stromal cell engulfment reveals metastatic advantage in breast cancer. Cell Rep. *27*, 3916–3926.e5. https://doi.org/10.1016/j.celrep.2019.05.084.

Ding, L., and Kleer, C.G. (2006). Enhancer of Zeste 2 as a marker of preneoplastic progression in the breast. Cancer Res. *66*, 9352–9355.

Ding, L., Erdmann, C., Chinnaiyan, A.M., Merajver, S.D., and Kleer, C.G. (2006). Identification of EZH2 as a molecular marker for a precancerous state in morphologically normal breast tissues. Cancer Res. *66*, 4095–4099.

Djomehri, S.I., Gonzalez, M.E., da Veiga Leprevost, F., Tekula, S.R., Chang, H.Y., White, M.J., Cimino-Mathews, A., Burman, B., Basrur, V., Argani, P., et al. (2020). Quantitative proteomic landscape of metaplastic breast carcinoma pathological subtypes and their relationship to triple-negative tumors. Nat. Commun. *11*, 1723. https://doi.org/10.1038/s41467-020-15283-z.

Dockerill, M., Gregson, C., and O' Donovan, D.H. (2021). Targeting PRC2 for the treatment of cancer: an updated patent review (2016 - 2020). Expert Opin. Ther. Pat. *31*, 119–135. https://doi.org/10.1080/13543776.2021.1841167.

Fiskus, W., Pranpat, M., Balasis, M., Herger, B., Rao, R., Chinnaiyan, A., Atadja, P., and Bhalla, K. (2006). Histone deacetylase inhibitors deplete enhancer of zeste 2 and associated polycomb repressive complex 2 proteins in human acute leukemia cells. Mol. Cancer Ther. *5*, 3096–3104. https://doi.org/10.1158/1535-7163.MCT-06-0418.

Gonzalez, M.E., DuPrie, M.L., Krueger, H., Merajver, S.D., Ventura, A.C., Toy, K.A., and Kleer, C.G. (2011). Histone methyltransferase EZH2 induces Akt-dependent genomic instability and BRCA1 inhibition in breast cancer. Cancer Res. *71*, 2360–2370. https://doi.org/10.1158/0008-5472.CAN-10-193371/6/2360.

Gonzalez, M.E., Li, X., Toy, K., DuPrie, M., Ventura, A.C., Banerjee, M., Ljungman, M., Merajver, S.D., and Kleer, C.G. (2009). Downregulation of EZH2 decreases growth of estrogen receptor-negative invasive breast carcinoma and requires BRCA1. Oncogene *28*, 843–853. https://doi.org/10.1038/onc.2008.433onc2008433.

Gonzalez, M.E., Moore, H.M., Li, X., Toy, K.A., Huang, W., Sabel, M.S., Kidwell, K.M., and Kleer, C.G. (2014). EZH2 expands breast stem cells through activation of NOTCH1 signaling. Proc. Natl. Acad. Sci. U. S. A. *111*, 3098–3103. https://doi.org/10.1073/pnas.1308953111113089531111.

Gounder, M., Schöffski, P., Jones, R.L., Agulnik, M., Cote, G.M., Villalobos, V.M., Attia, S., Chugh, R., Chen, T.W.W., Jahan, T., et al. (2020). Tazemetostat in advanced epithelioid sarcoma with loss of INI1/SMARCB1: an international, open-label, phase 2 basket study. Lancet Oncol. *21*, 1423–1432. https://doi.org/10.1016/S1470-2045(20)30451-4.

Gui, J., Zahedi, F., Ortiz, A., Cho, C., Katlinski, K.V., Alicea-Torres, K., Li, J., Todd, L., Zhang, H., Beiting, D.P., et al. (2020). Activation of p38alpha stress-activated protein kinase drives the formation of the pre-metastatic niche in the lungs. Nat. Cancer *1*, 603–619. https://doi.org/10.1038/s43018-020-0064-0.

Gulati, N., Béguelin, W., and Giulino-Roth, L. (2018). Enhancer of zeste homolog 2 (EZH2) inhibitors. Leuk. Lymphoma *59*, 1574–1585. https://doi.org/10.1080/10428194.2018.1430795.

Hoffmeyer, K., Junghans, D., Kanzler, B., and Kemler, R. (2017). Trimethylation and acetylation of beta-catenin at lysine 49 represent key elements in ESC pluripotency. Cell Rep. *18*, 2815–2824. https://doi.org/10.1016/j.celrep.2017.02.076.

Hoy, S.M. (2020). Tazemetostat: first approval. Drugs *80*, 513–521. https://doi.org/10.1007/s40265-020-01288-x.

Hua, W.K., Chang, Y.I., Yao, C.L., Hwang, S.M., Chang, C.Y., and Lin, W.J. (2013). Protein arginine methyltransferase 1 interacts with and activates p38alpha to facilitate erythroid differentiation. PLoS One *8*, e56715. https://doi.org/10.1371/journal.pone.0056715.

Huang, J., Perez-Burgos, L., Placek, B.J., Sengupta, R., Richter, M., Dorsey, J.A., Kubicek, S., Opravil, S., Jenuwein, T., and Berger, S.L. (2006). Repression of p53 activity by Smyd2-mediated methylation. Nature *444*, 629–632. https://doi.org/10.1038/nature05287.

Ianevski, A., He, L., Aittokallio, T., and Tang, J. (2017). SynergyFinder: a web application for analyzing drug combination dose-response matrix data. Bioinformatics *33*, 2413–2415. https://doi.org/10.1093/bioinformatics/btx162.

Igea, A., and Nebreda, A.R. (2015). The stress kinase p38alpha as a target for cancer therapy. Cancer Res. 0008–5472. https://doi.org/10.1158/0008-5472.

Italiano, A., Soria, J.C., Toulmonde, M., Michot, J.M., Lucchesi, C., Varga, A., Coindre, J.M., Blakemore, S.J., Clawson, A., Suttle, B., et al. (2018). Tazemetostat, an EZH2 inhibitor, in relapsed or refractory B-cell non-Hodgkin lymphoma and advanced solid tumours: a first-in-human, open-label, phase 1 study. Lancet Oncol. *19*, 649–659. https://doi.org/10.1016/S1470-2045(18)30145-1.

Jeong, H.J., Lee, S.J., Lee, H.J., Kim, H.B., Anh Vuong, T., Cho, H., Bae, G.U., and Kang, J.S. (2020). Prmt7 promotes myoblast differentiation via methylation of p38MAPK on arginine residue 70. Cell Death Differ. *27*, 573–586. https://doi.org/10.1038/s41418-019-0373-y.

Kim, E., Kim, M., Woo, D.H., Shin, Y., Shin, J., Chang, N., Oh, Y.T., Kim, H., Rheey, J., Nakano, I., et al. (2013). Phosphorylation of EZH2 activates STAT3 signaling via STAT3 methylation and promotes tumorigenicity of glioblastoma stem-like cells. Cancer Cell *23*, 839–852. https://doi.org/10.1016/j.ccr.2013.04.008S1535-6108(13)00177-3.

Kim, K.H., and Roberts, C.W.M. (2016). Targeting EZH2 in cancer. Nat. Med. *22*, 128–134. https://doi.org/10.1038/nm.4036.

Kleer, C.G., Cao, Q., Varambally, S., Shen, R., Ota, I., Tomlins, S.A., Ghosh, D., Sewalt, R.G.A.B., Otte, A.P., Hayes, D.F., et al. (2003). EZH2 is a marker of aggressive breast cancer and promotes neoplastic transformation of breast epithelial cells. Proc. Natl. Acad. Sci. USA. *100*, 11606–11611. https://doi.org/10.1073/pnas.1933744100.

Knutson, S.K., Kawano, S., Minoshima, Y., Warholic, N.M., Huang, K.C., Xiao, Y., Kadowaki, T., Uesugi, M., Kuznetsov, G., Kumar, N., et al. (2014). Selective inhibition of EZH2 by EPZ-6438 leads to potent antitumor activity in EZH2-mutant non-Hodgkin lymphoma. Mol. Cancer Ther. *13*, 842–854. https://doi.org/10.1158/1535-7163.MCT-13-0773.

Kuzmichev, A., Jenuwein, T., Tempst, P., and Reinberg, D. (2004). Different EZH2-containing complexes target methylation of histone H1 or nucleosomal histone H3. Mol. Cell *14*, 183–193.

Lee, T.I., Jenner, R.G., Boyer, L.A., Guenther, M.G., Levine, S.S., Kumar, R.M., Chevalier, B., Johnstone, S.E., Cole, M.F., Isono, K.i., et al. (2006). Control of developmental regulators by Polycomb in human embryonic stem cells. Cell *125*, 301–313. https://doi.org/10.1016/j.cell.2006.02.043.

Liu, M.Y., Hua, W.K., Chen, C.J., and Lin, W.J. (2020). The MKK-dependent phosphorylation of p38alpha is augmented by arginine methylation on arg49/arg149 during erythroid differentiation. Int. J. Mol. Sci. *21*, E3546. https://doi.org/10.3390/ijms21103546.

Lu, T., Jackson, M.W., Wang, B., Yang, M., Chance, M.R., Miyagi, M., Gudkov, A.V., and Stark, G.R. (2010). Regulation of NF-kappaB by NSD1/FBXL11-dependent reversible lysine methylation of p65. Proc. Natl. Acad. Sci. USA. *107*, 46–51. https://doi.org/10.1073/pnas.0912493107.

Margueron, R., and Reinberg, D. (2011). The Polycomb complex PRC2 and its mark in life. Nature *469*, 343–349. https://doi.org/10.1038/nature09784.

Martin, E.E., Huang, W., Anwar, T., Arellano-Garcia, C., Burman, B., Guan, J.L., Gonzalez, M.E., and Kleer, C.G. (2017). MMTV-cre;Ccn6 knockout mice develop tumors recapitulating human metaplastic breast carcinomas. Oncogene *36*, 2275–2285. https://doi.org/10.1038/onc.2016.381onc2016381.

McGuire, A., Lowery, A.J., Kell, M.R., Kerin, M.J., and Sweeney, K.J. (2017). Locoregional recurrence following breast cancer surgery in the trastuzumab era: a systematic review by subtype. Ann. Surg. Oncol. *24*, 3124–3132. https://doi.org/10.1245/s10434-017-6021-1.

McHugh, J.B., Fullen, D.R., Ma, L., Kleer, C.G., and Su, L.D. (2007). Expression of polycomb group protein EZH2 in nevi and melanoma. J. Cutan. Pathol. *34*, 597–600. https://doi.org/10.1111/j.1600-0560.2006.00678.x.

McMullen, E.R., Skala, S.L., Gonzalez, M.E., Djomehri, S., Chandrashekar, D.S., Varambally, S., and Kleer, C.G. (2021). Subcellular localization of EZH2 phosphorylated at T367 stratifies metaplastic breast carcinoma subtypes. Breast Cancer *28*, 496–505. https://doi.org/10.1007/s12282-020-01189-7.

Moore, H.M., Gonzalez, M.E., Toy, K.A., Cimino-Mathews, A., Argani, P., and Kleer, C.G. (2013). EZH2 inhibition decreases p38 signaling and suppresses breast cancer motility and metastasis. Breast Cancer Res. Treat. *138*, 741–752. https://doi.org/10.1007/s10549-013-2498-x.

Morey, L., and Helin, K. (2010). Polycomb group protein-mediated repression of transcription. Trends Biochem. Sci. *35*, 323–332. https://doi.org/10.1016/j.tibs.2010.02.009.

Nguyen, T., Ruan, Z., Oruganty, K., and Kannan, N. (2015). Co-conserved MAPK features couple D-domain docking groove to distal allosteric sites via the C-terminal flanking tail. PLoS One *10*, e0119636.

Nie, L., Wei, Y., Zhang, F., Hsu, Y.H., Chan, L.C., Xia, W., Ke, B., Zhu, C., Deng, R., Tang, J., et al. (2019). CDK2-mediated site-specific phosphorylation of EZH2 drives and maintains triple-negative breast cancer. Nat. Commun. *10*, 5114. https://doi.org/10.1038/s41467-019-13105-5.

Nie, L., Wei, Y., Zhang, F., Hsu, Y.H., Chan, L.C., Xia, W., Ke, B., Zhu, C., Deng, R., Tang, J., et al. (2020). Author Correction: CDK2-mediated site-specific phosphorylation of EZH2 drives and maintains triple-negative breast cancer. Nat. Commun. *11*, 673. https://doi.org/10.1038/s41467-020-14429-3.

Palacios, D., Mozzetta, C., Consalvi, S., Caretti, G., Saccone, V., Proserpio, V., Marquez, V.E., Valente, S., Mai, A., Forcales, S.V., et al. (2010). TNF/p38alpha/polycomb signaling to Pax7 locus in satellite cells links inflammation to the epigenetic control of muscle regeneration. Cell Stem Cell *7*, 455–469. https://doi.org/10.1016/j.stem.2010.08.013S1934-5909(10)00435-2.

Pang, J., Toy, K.A., Griffith, K.A., Awuah, B., Quayson, S., Newman, L.A., and Kleer, C.G. (2012). Invasive breast carcinomas in Ghana: high frequency of high grade, basal-like histology and high EZH2 expression. Breast Cancer Res. Treat. *135*, 59–66. https://doi.org/10.1007/s10549-012-2055-z.

Pascual, J., and Turner, N.C. (2019). Targeting the PI3-kinase pathway in triple-negative breast cancer. Ann. Oncol. *30*, 1051–1060. https://doi.org/10.1093/annonc/mdz133.

Patnaik, A., Haluska, P., Tolcher, A.W., Erlichman, C., Papadopoulos, K.P., Lensing, J.L., Beeram, M., Molina, J.R., Rasco, D.W., Arcos, R.R., et al. (2016). A first-in-human phase I study of the oral p38 MAPK inhibitor, ralimetinib (LY2228820 dimesylate), in patients with advanced cancer. Clin. Cancer Res. *22*, 1095–1102. https://doi.org/10.1158/1078-0432.CCR-15-1718.

Pereira, L., Igea, A., Canovas, B., Dolado, I., and Nebreda, A.R. (2013). Inhibition of p38 MAPK sensitizes tumour cells to cisplatin-induced apoptosis mediated by reactive oxygen species and JNK. EMBO Mol. Med. *5*, 1759–1774. https://doi.org/10.1002/emmm.201302732.

Raaphorst, F.M., Meijer, C.J.L.M., Fieret, E., Blokzijl, T., Mommers, E., Buerger, H., Packeisen, J., Sewalt, R.A.B., Otte, A.P., and van Diest, P.J. (2003). Poorly differentiated breast carcinoma is associated with increased expression of the human polycomb group EZH2 gene. Neoplasia 5, 481–488.

Raaphorst, F.M., van Kemenade, F.J., Blokzijl, T., Fieret, E., Hamer, K.M., Satijn, D.P., Otte, A.P., and Meijer, C.J. (2000). Coexpression of BMI-1 and EZH2 polycomb group genes in Reed-Sternberg cells of Hodgkin's disease. Am. J. Pathol. *157*, 709–715.

Richly, H., Aloia, L., and Di Croce, L. (2011). Roles of the Polycomb group proteins in stem cells and cancer. Cell Death Dis. *2*, e204. https://doi.org/10.1038/cddis.2011.84.

Sarkozy, C., Morschhauser, F., Dubois, S., Molina, T., Michot, J.M., Cullières-Dartigues, P., Suttle, B., Karlin, L., Le Gouill, S., Picquenot, J.M., et al. (2020). A LYSA Phase Ib Study of Tazemetostat (EPZ-6438) plus R-CHOP in Patients with Newly Diagnosed Diffuse Large B-Cell Lymphoma (DLBCL) with Poor Prognosis Features. Clin. Cancer Res. *26*, 3145–3153. https://doi.org/10.1158/1078-0432.CCR-19-3741.

Shen, X., Liu, Y., Hsu, Y.J., Fujiwara, Y., Kim, J., Mao, X., Yuan, G.C., and Orkin, S.H. (2008). EZH1 mediates methylation on histone H3 lysine 27 and complements EZH2 in maintaining stem cell identity and executing pluripotency. Mol. Cell *32*, 491–502. https://doi.org/10.1016/j.molcel.2008.10.016.

Siegel, R.L., Miller, K.D., and Jemal, A. (2018). Cancer statistics, 2018. CA. Cancer J. Clin. *68*, 7–30. https://doi.org/10.3322/caac.21442.

Simon, J.A., and Kingston, R.E. (2009). Mechanisms of polycomb gene silencing: knowns and unknowns. Nat. Rev. Mol. Cell Biol. *10*, 697–708. https://doi.org/10.1038/nrm2763.

Sparmann, A., and van Lohuizen, M. (2006). Polycomb silencers control cell fate, development and cancer. Nat. Rev. Cancer *6*, 846–856. https://doi.org/10.1038/nrc1991.

Stark, G.R., Wang, Y., and Lu, T. (2011). Lysine methylation of promoter-bound transcription factors and relevance to cancer. Cell Res. *21*, 375–380. https://doi.org/10.1038/cr.2010.174.

Sudo, T., Utsunomiya, T., Mimori, K., Nagahara, H., Ogawa, K., Inoue, H., Wakiyama, S., Fujita, H., Shirouzu, K., and Mori, M. (2005). Clinicopathological significance of EZH2 mRNA expression in patients with hepatocellular carcinoma. Br. J. Cancer *92*, 1754–1758.

Vagia, E., Mahalingam, D., and Cristofanilli, M. (2020). The landscape of targeted therapies in TNBC. Cancers (Basel) *12*, E916. https://doi.org/10.3390/cancers12040916.

Varambally, S., Dhanasekaran, S.M., Zhou, M., Barrette, T.R., Kumar-Sinha, C., Sanda, M.G., Ghosh, D., Pienta, K.J., Sewalt, R.G.A.B., Otte, A.P., et al. (2002). The polycomb group protein EZH2 is involved in progression of prostate cancer. Nature *419*, 624–629.

Visser, H.P., Gunster, M.J., Kluin-Nelemans, H.C., Manders, E.M., Raaphorst, F.M., Meijer, C.J., Willemze, R., and Otte, A.P. (2001). The Polycomb group protein EZH2 is upregulated in proliferating, cultured human mantle cell lymphoma. Br. J. Haematol. *112*, 950–958.

Wagner, E.F., and Nebreda, A.R. (2009). Signal integration by JNK and p38 MAPK pathways in cancer development. Nat. Rev. Cancer *9*, 537–549. https://doi.org/10.1038/nrc2694nrc2694.

Wu, X., Zhang, W., Font-Burgada, J., Palmer, T., Hamil, A.S., Biswas, S.K., Poidinger, M., Borcherding, N., Xie, Q., Ellies, L.G., et al. (2014). Ubiquitin-conjugating enzyme Ubc13 controls breast cancer metastasis through a TAK1-p38 MAP kinase cascade. Proc. Natl. Acad. Sci. USA. *111*, 13870–13875. https://doi.org/10.1073/pnas.1414358111414358111.

Xu, K., Wu, Z.J., Groner, A.C., He, H.H., Cai, C., Lis, R.T., Wu, X., Stack, E.C., Loda, M., Liu, T., et al. (2012). EZH2 oncogenic activity in castration-resistant prostate cancer cells is Polycomb-independent. Science *338*, 1465–1469. https://doi.org/10.1126/science.1227604338/6113/1465.

Yang, J., Huang, J., Dasgupta, M., Sears, N., Miyagi, M., Wang, B., Chance, M.R., Chen, X., Du, Y., Wang, Y., et al. (2010). Reversible methylation of promoter-bound STAT3 by histone-modifying enzymes. Proc. Natl. Acad. Sci. USA. *107*, 21499–21504. https://doi.org/10.1073/pnas.1016147107.

Yomtoubian, S., Lee, S.B., Verma, A., Izzo, F., Markowitz, G., Choi, H., Cerchietti, L., Vahdat, L., Brown, K.A., Andreopoulou, E., et al. (2020). Inhibition of EZH2 catalytic activity selectively targets a metastatic subpopulation in triple-negative breast cancer. Cell Rep. *30*, 755–770.e6. https://doi.org/10.1016/j.celrep.2019.12.056.

Zarubin, T., and Han, J. (2005). Activation and signaling of the p38 MAP kinase pathway. Cell Res. *15*, 11–18. https://doi.org/10.1038/sj.cr.7290257.

STAR★METHODS

KEY RESOURCES TABLE

REAGENT or RESOURCE	SOURCE	IDENTIFIER
Antibodies		
Rabbit polyclonal anti-Methylated Lysine	Sigma-Aldrich	Cat #SAB5200093
Rabbit Monoclonal anti-p38 MAPK	Cell Signaling	Cat #8690; RRID:AB_10999090
Rabbit Monoclonal anti-EZH2	Cell Signaling	Cat #5246; RRID:AB_10694683
Rabbit Monoclonal anti- phospho-p38 MAPK (Thr180/Tyr182)	Cell Signaling	Cat #4511; RRID:AB_2139682
Rabbit Monoclonal anti-Myc tag	Cell Signaling	Cat #2278S; RRID:AB_490778
Mouse Monoclonal anti-alpha-Tubulin	Sigma-Aldrich	Cat #T9026; RRID:AB_477593
Rabbit Monoclonal anti-phospho-Hsp27 (Ser82)	Cell Signaling	Cat #9709S; RRID:AB_11217429
Rabbit Monoclonal anti-Hsp27	Cell Signaling	Cat #95357S; RRID:AB_2800246
Rabbit polyclonal anti-Histone H3	Cell Signaling	Cat #9715; RRID:AB_331563
Rabbit Monoclonal anti-trimethyl-Histone H3 (Lys27)	Cell Signaling	Cat #9733; RRID:AB_2616029
Rabbit Monoclonal anti-MKK6	Cell Signaling	Cat #8550; RRID:AB_11220227
Rabbit Monoclonal anti-HA-Tag	Cell Signaling	Cat #3724; RRID:AB_1549585
Mouse Monoclonal anti-beta-Actin	Santa-Cruz Biotechnology	Cat #Sc-47778; RRID:AB_626632
Rabbit Polyclonal anti-Lamin B1	Abcam	Cat #AB16048; RRID:AB_443298
Mouse Monoclonal anti-GAPDH	Abcam	Cat #AB9484; RRID:AB_307274
Rabbit Monoclonal anti-Phospho-Akt (Ser473)	Cell Signaling	Cat #4060; RRID:AB_2315049
Rabbit Monoclonal anti-Akt	Cell Signaling	Cat #4691; RRID:AB_915783
Rabbit Monoclonal anti-phospho-Akt1/PKBa (Rac) (Ser 473)	Cell Signaling	Cat #9018; RRID:AB_2629283
Rabbit Monoclonal anti-Akt1	Cell Signaling	Cat #2938; RRID:AB_915788
Rabbit Monoclonal anti-Cytokeratin 14	Abcam	Cat #ab119695; RRID:AB_10898957
Rabbit Monoclonal anti-Cytokeratin 18	Abcam	Cat #ab133263; RRID:AB_11155892
Rabbit Anti-pEZH2	Pierce	Custom antibody
Mouse Monoclonal anti-p38 MAPK alpha	Invitrogen	Cat #MA5-15116
Rabbit monoclonal anti-ubiquitin	Cell Signaling	Cat #43124S; RRID:AB_2799235
Mouse monoclonal anti-EED	Abcam	Cat #ab126542
Rabbit polyclonal anti-EED	Abcam	Cat #ab4469
Rabbit Monoclonal anti-SUZ12	Cell Signaling	Cat #3737
Bacterial and virus strains		
Lentivirus	University of Michigan, Biomedical Research core Facilities (Vector core)	N/A
Biological samples		
Human tumor samples	University of Michigan and Johns Hopkins	(Kleer et al., 2003; Moore et al., 2013)
Xenografts derived from MDA-MB-231	University of Michigan (Kleer Laboratory)	This paper
Xenografts derived from 4T1	University of Michigan (Kleer Laboratory)	This paper
Chemicals, peptides, and recombinant proteins		
GSK-343	Sigma-Aldrich	Cat # SML0766
SB202190	Cell Signaling	Cat #81585
EPZ-6438 50 mg	Selleck Chemicals	Cat #S7128
Cycloheximide solution 1 mL	Sigma-Aldrich	Cat #C4859

(*Continued on next page*)

Continued

REAGENT or RESOURCE	SOURCE	IDENTIFIER
MAPK14 (p38α), His-Tag	BPS Bioscience	Cat #40243
MG-132	Cell Signaling	Cat #2194S
Doxycycline	Sigma Aldrich	Cat #D3072
Recombinant Histone H3	BPS Bioscience	Cat #79055-2
Recombinant GST-p38α	BPS Bioscience	Cat #40070
Recombinant GST-EZH2	BPS Bioscience	Cat #50279
Recombinant PRC2 complex	BPS Bioscience	Cat #51004
Critical commercial assays		
Duolink *In Situ* Red Starter Kit Mouse/Rabbit	Sigma-Aldrich	Cat #DUO92101
MTase-Glo™ Methyltransferase Assay	Promega	Cat #V7601
Hoescht 33258	Thermo Fisher Scientific	Cat # H1398
Annexin V Staining	Thermo Fisher Scientific	Cat #A13201
Deposited data		
RNA sequencing	Advanced Genomics Core University of Michigan	GSE207795
ChIP sequencing	Advanced Genomics core University of Michigan	GSE207794
Experimental models: Cell lines		
Human: MDA-MB-231	ATCC	CRM-HTB-26
Murine: 4T1	ATCC	CRL-2539; RRID:CVCL_0125
Human: Patient-derived TNBC cells T4	University of Michigan (Kleer Laboratory)	(Gonzalez et al., 2014)
Human: Patient-derived TNBC cells Vari068	University of Michigan (Merajver Laboratory)	N/A
Human: SUM149	University of Michigan (Ethier Laboratory)	N/A
Murine: *Ccn6*$^{fl/fl}$ from MMTV-Cre;*Ccn6*$^{fl/fl}$ mouse TNBC metaplastic carcinomas	University of Michigan (Kleer Laboratory)	(Martin et al., 2017)
Experimental models: Organisms/strains		
Mouse: NOD/SCID (NSG)	Jackson Laboratory	Cat #005557
Mouse: BALB/c mice	Jackson Laboratory	Cat #000651
Mouse: Nude athymic mice	Jackson Laboratory	Cat #002019
Oligonucleotides		
Primers: HAp38α K139A: Forward 5′-aattatgtcagctgaatgtatat acgctagacctcggagaatttggtagata-3′ Reverse 5′-tatctaccaaattctccgaggt ctagcgtatatacattcagctgacataatt-3′	Thermo Fisher Scientific	This paper
Primers: HAp38α K165A: Forward 5′-tgaatgaagactgtga gctggcgattctggattttggactgg-3′, Reverse 5′-ccagtccaaaatccaga atcgccagctcacagtcttcattca-3′	Thermo Fisher Scientific	This paper
ShRNA EZH2 (1)	Sigma Aldrich	TRCN0000286227
shRNA EZH2 (2)	Sigma Aldrich	TRCN0000353069
Recombinant DNA		
Plasmid: pBabe pSLIK 3xHA-MKK6-EE neo	Addgene	#47546
Plasmid: pBabe-myc-EZH2 (wild-type)	Dulbecco Telethon Institute (DTI), IRCCS Fondazione Santa Lucia and European Brain Research Institute. Puri Laboratory	(Palacios et al., 2010)

(*Continued on next page*)

Continued

REAGENT or RESOURCE	SOURCE	IDENTIFIER
Plasmid: pBabe-myc-EZH2 (T367A)	Dulbecco Telethon Institute (DTI), IRCCS Fondazione Santa Lucia and European Brain Research Institute. Puri Laboratory	(Palacios et al., 2010)
Software and algorithms		
ImageJ	https://imagej.nih.gov/ij/	https://imagej.nih.gov/ij/
Advaita iPathwayguide	https://ipathwayguide.advaitabio.com/dashboard	https://ipathwayguide.advaitabio.com/dashboard
GraphPad Prism 7	https://www.graphpad.com/guides/prism/7/user-guide/graphs2.htm	https://www.graphpad.com
SynergyFinder	(Ianevski et al., 2017)	https://synergyfinder.fimm.fi

RESOURCE AVAILABILITY

Lead contact

Further information and requests for resources and reagents should be directed to and will be fulfilled by the Lead Contact, Dr. Celina Kleer (kleer@umich.edu).

Materials availability

All reagents generated in this study, including p38 methyl mutants are available upon request to the lead contact.

Data and code availability

RNA-Seq and ChIP-Seq datasets have been deposited at GEO and are publicly available as of the date of publication. Accession numbers are listed in the key resources table. The paper does not report original code.

EXPERIMENTAL MODEL AND SUBJECT DETAILS

Tissue samples and immunohistochemistry

The use of human tissue samples for this study was approved by the Institutional Review Board of the University of Michigan. We employed two independent cohorts of human tissue samples arranged in TMAs including i). Sixteen primary breast carcinomas and matched metastasis from the same patients, and ii). Ninety-four primary invasive carcinomas. The clinicopathological characteristics and p-p38 expression of these cohorts have been previously reported (Kleer et al., 2003; Moore et al., 2013). Five-micron thick sections of the TMAs as well as mouse tumors, lungs, and bones of mice were collected, fixed in 10% neutral buffered formalin, and embedded in paraffin for immunohistochemistry. Primary antibodies used included anti-pEZH2-T367 developed and validated in our lab (Anwar et al., 2018), phospho-p38 MAPK (Cell Signaling #4511), phospho-AKT1 (Ser473) (rabbit polyclonal, Millipore, Cat# 07–310, and cytokeratin-18 (Abcam, #ab133263). pEZH2-T367, phospho-p38, and phospho-AKT1 were scored as high when >10% of the cancer cells showed moderate or strong staining and were scored as low when staining was present in <10% of tumor cells based on our previous studies. Two tailed Fisher's exact and chi square tests were performed to analyze the association between pEZH2-T367 and pAKT1 and between pEZH2-T367 and phospho-p38 proteins. A p value < 0.05 was considered significant.

Animal studies

The animal studies in this study were approved by the UCUCA of the University of Michigan. Eight-week-old severe combined immunodeficiency female mice (NOD/SCID, The Jackson Laboratory) were used for examining tumorigenicity, as previously reported (Anwar et al., 2018). Briefly, MDA-MB-231 cells were orthotopically injected into the right inguinal mammary fat pad of anesthetized mice at a concentration of 2 x10^6 cells resuspended in 50 µL of Matrigel (n = 10 mice per group). When tumors reached 100 mm^3 mice were treated 5 days/weeks by intraperitoneal (i.p.) injection with 4% DMSO-30% PEG 300-5% Tween 80 (control), SB202190 (1 mg/kg/day), EPZ-6438 (10 mg/kg/day) or a combination of

SB202190 and EPZ-6438. Primary tumor growth was monitored biweekly by caliper measurements. All mice were sacrificed when the first primary tumor reached 2 cm^3. At the time of necropsy, the primary tumor, lung, and sites of metastasis were harvested and subjected to histopathology. The primary tumors were also employed for Western blot, Co-IPs, RNA sequencing studies, and immunohistochemistry.

4T1 cells were injected orthotopically in the fourth mammary gland of female BALB/c mice (The Jackson Laboratory) at a concentration of 2.5 x10^5 cells. When tumors reached 100 mm^3, mice were treated as described above. Mice were euthanized when tumors reached 2cm^3 and subjected to necropsy. Primary tumors were analyzed by histopathology, WB, and co-IPs.

For the lung colonization studies, female nude athymic mice (n = 10 per group) were injected intracardially with MDA-MB-231 2x10^5 cells and treated with 4% DMSO-30% PEG 300-5% Tween 80 (control), SB202190 (1 mg/kg/day), EPZ-6438 (10 mg/kg/day) or the combination of p38 and EPZ-6438 5 times per week for 3 weeks. Mice were then euthanized and the presence of metastasis was verified by histopathology.

METHOD DETAILS

Cell culture and transductions

Breast cancer cell lines MDA-MB-231 and murine 4T1 cells were purchased from the American Type Culture Collection and grown under recommended conditions. T4 and Vari068 primary breast cancer cells were derived from fresh patients' tumors and maintained as previously reported (Gonzalez et al., 2014). MMTV-Cre;*Ccnδ*$^{fl/fl}$ metaplastic breast carcinoma cells were derived from primary mouse mammary carcinomas in this model (Martin et al., 2017). Cell lines were authenticated using STR profiling and were tested for mycoplasma infection using Sigma LookOut Mycoplasma PCR Detection Kit (Cat MP0035).

EZH2 knockdown and rescue was carried out using lentiviral transduction of EZH2 with pBabe-myc-EZH2 (wild-type) or pBabe-myc-EZH2 (T367A) as described in (Anwar et al., 2018). After transduction, cells were selected for antibiotic resistant with 2 μg mL^{-1}puromycin (Sigma Aldrich, #P9620), followed by knockdown using stable short-hairpin interfering RNA (MISSION shRNA, Sigma Aldrich) targeting the 3′UTR of Ezh2 (TRCN0000286227), as previously reported (Gonzalez et al., 2011). Oligos in the pLKO.1 vector were packaged into lentiviral particles at the University of Michigan Vector Core.

We performed mutagenesis assays to replace K165 and K139 for alanine and developed single as well as double mutants of p38α. Primers used for mutagenesis reactions to create HA-p38a K139A, HA-p38a K165A, and HA-p38a K130A/K165K constructs from HA-p38a are: K139A: Forward 5′-AATTATGTCAGCT GAATGTATATACGCTAGACCTCGGAGAATTTGGTAGATA-3′, Reverse 5′-TATCTACCAAATTCTCCGAG GTCTAGCGTATATACATTCAGCTGACATAATT-3′; K165A:

Forward 5′TGAATGAAGACTGTGAGCTGGCGATTCTGGATTTTGGACTGG-3′,

Reverse 5′CCAGTCCAAAATCCAGAATCGCCAGCTCACAGTCTTCATTCA-3′.

Inducible activation of p38 MAPK was used using the pBabe pSLIK 3xHA-MKK6-EE neo plasmid, a kind gift from Kevin Janes (Addgene plasmid #47546). Cells were transduced with lentivirus and selected with Geneticin (Gibco #10131) and treated with 2 μg mL^{-1} doxycycline (Sigma Aldrich, #D3072) to induce MKK6 activation (Palacios et al., 2010).

Western blot, immunoprecipitation, and protein stability assay

Immunoblots were carried out using 50 μg of whole cell extract, as previously reported (Gonzalez et al., 2011). Briefly, cells were lysed in RIPA lysis buffer (Pierce #89900) with protease and phosphatase inhibitors (Thermo Scientific #1861281). Samples were resolved by SDS–PAGE, transferred onto PVDF membranes, and membranes were blocked and incubated with primary antibodies in 5% BSA (Sigma Aldrich, #A3059) in TBS-T (Bio-Rad, #161-0372 with 0.05% Tween 20) or 5% milk (Bio-Rad #170-6404) in TBS-T at 4°C overnight. Protein signals were detected using enhanced chemiluminescence (Pierce, #32106) as per the manufacturer's instructions. Primary antibodies used included anti-pEZH2-T367 developed and validated in our lab (Anwar et al., 2018), Cell Signaling antibodies: EZH2 (#5246), Histone H3 (#9715), Myc-tag (#2276), p38α (#9218), trimethyl-histone H3 (Lys27) (#9733), AKT (pan) (#4691), phospho-p38 (#4511), phospho-Hsp27 (#2401), phospho-AKT (Ser473) (D9E, #4060), phospho-AKT1/PKBa (Ser473)

(#9018). Abcam antibodies: CK18 (#ab133263) and CK14 (#ab119695). Sigma-Aldrich antibodies: alpha-tubulin (#T9026), methyl-K (#SAB5200093). β-Actin HRP (Santa Cruz, #sc47778) was used as for loading control. Secondary antibodies used were Amersham ECL anti-rabbit IgG HRP-linked (GE Healthcare Life Sciences, #NA934) or Amersham ECL anti-mouse IgG HRP-linked (GE Healthcare Life Sciences, #NA931).

Immunoprecipitations of endogenous proteins was performed using magnetic Dynabeads following protocol instructions (Invitrogen, #10007D) as we have reported previously (Anwar et al., 2018). Antibodies used for immunoprecipitation included p38α, phospho-p38, and methyl-K. The stability of p38α and EZH2 proteins was ascertained using 100 μg/mL cycloheximide pulse-chase treatment for 0, 3, 6, 9, and 18 h. For ubiquitination assays, MDA-MB-231 cells were transduced with HA-p38α K139A, HA-p38α K165A, and HA-p38α K130A/K165K constructs and treated for 5 h with the proteasome inhibitor MG-132 50 μg. Whole cell extracts were immunoprecipitated by anti-magnetics A beads followed by immunoblot using antibodies against ubiquitin, p-p38, *p*-Hsp27, Hsp27, p38α. Vehicle treated lysates were used as loading control.

Lysine methyltransferase assay

EZH2 lysine N-methyltransferase (KMTase) activity was evaluated with a bioluminescence-based assay determining S-adenosyl homocysteine (SAH) production using MTaseGlo Methyltransferase assay (Promega, Cat #V7601). Whole cell extract of MDA-MB-231, T4, and Vari068 cells was diluted with 1X Reaction Buffer (20 mM Tris buffer, pH 8.0, 50 mM NaCl, 1 mM EDTA, 3 mM $MgCl_2$, 0.1 mg/mL BSA, 1 mM dithiothreitol (DTT)) and incubated with a substrate solution containing 10 μM S-adenosyl-methionine (SAM) and 0.1 mg/mL of human recombinant p38α (BPS, Bioscience, Cat # 40243) in a 96-well solid white plate. The enzyme reaction was carried out for 1 h at room temperature (23°C). Upon completion of the reaction, 5 μL of MTase-Glo Reagent was added to convert SAH to ADP for 30 min at room temperature. Finally, 25 μL of MTase-Glo Detection Reagent was added and incubated for 30 min at room temperature to convert ADP to ATP, which was detected via a luciferase reaction using a BioTek SYNERGY H1 microplate reader.

LC-MS/MS analyses of methylated proteins

Recombinant histone H3 and GST-p38α were each incubated with or without recombinant PRC2 complex (EZH2/EED/SUZ12/RbAp48/AEBP2) and S-adenosyl methionine methyl donor in sodium phosphate-buffered HMTase buffer solution for one hour at 37°C. Samples were subsequently run on a gel and digested in-gel using trypsin or Arg-C and analyzed for mono, di, and trimethylation by LC-MS/MS at the University of Michigan Proteomics Core. Methylation was confirmed by γ and β-ion.

Inhibitors and synergy score calculation

The EZH2 methyltransferase inhibitors GSK-343 (Sigma-Aldrich, #SML0766) and EPZ-6438 (Selleckchem, #S7128), and p38 inhibitor SB202190 (Cell Signaling #8158) were used. MDA-MB-231 and SUM149 cells were treated with GSK-343 (1, 2, 3, 5 and 8 μM) and SB202190 (5, 10, 20, 30 and 40 μM) or a combination of GSK-343 and SB202190 for 96 h respectively. Cell viability measurements were used for calculating IC50. Data were analyzed using GraphPad Prism 7 using nonlinear regression. Drug-drug interactions were quantified via SynergyFinder 2.0 (https://synergyfinder.fimm.fi) (Ianevski et al., 2017). In this method, a synergy score less than −10 denotes an antagonistic interaction, from −10 to 10 an additive interaction, and larger than 10 a synergistic interaction. Synergy summary scores were calculated across all the tested concentration combinations. To quantify the degree of drug synergy it has been used the Zero interaction potency (ZIP) model (https://www.ncbi.nlm.nih.gov/pmc/articles/PMC4759128). Based on these assays, we selected doses within the synergy range of the combination treatment for functional studies.

Wound healing, invasion, migration, proliferation, and apoptosis assays

GSK-343 and EPZ-6438 were used *in vitro* at 3 μM for 48 h, and at 20 μM for 48 h, respectively. SB202190 (Cell Signaling #8158) was used at 20 μM for 48 h as previously reported (Moore et al., 2013), and based on our viability and synergy assays. Wound healing assays were performed by seeding cells in complete media a 6-well plate for 24–48 h until a confluent monolayer had formed. Linear scratches were made using a sterile 200 μL pipette tip. Monolayers were washed three times with PBS to remove detached cells, and then complete media was added. Photographs of the wound were taken immediately after wound formation and 24 h after with phase contrast microscopy. Wound area was measured over time using ImageJ.

In vitro invasion assays were performed using a 24-well Matrigel invasion chamber (BD Biosciences, #354480), per manufacturer's instructions. All invasion experiments were performed with technical triplicates and repeated at least three times with biological replicates. Cells that had invaded through the Matrigel membrane were fixed with methanol, stained with crystal violet, photographed at high resolution, and counted manually using ImageJ. The representative whole inserts were imaged under the same conditions and are shown in this paper after increasing brightness by 20% across all images in Microsoft PowerPoint.

Microfluidic migration assays were performed using a previously published microfluidic migration platform (Chen et al., 2015, 2019). The bottom and top of the box are the first and third quartiles, and the band inside the box is always the second quartile (the median). The ends of the whiskers represent the 5th percentile and the 95th percentile. The square inside the box indicates the mean, and the *x* outside the box indicates the minimum and maximum of all the data.

Cell proliferation was determined using the Hoescht 33258 assay (Thermo Fisher, #H1398) and apoptosis was measured using Annexin V staining (Thermo Fisher, #A13201), following manufacturer's instructions.

Proximity ligation assays

Proximity ligation assay was carried out using Duolink detection reagent kit (Sigma-Aldrich, Cat #DUO92101). Cells were seeded in 8-well chambered slides (Thermo Fisher Lab-Tek Cat #154534) and after 48 h were fixed with 4% PFA in PBS for 15 min at room temperature. After three PBS washes, the cells were incubated with blocking buffer (5% normal goat serum containing 0.3% Triton X-100 in PBS) for one hour at room temperature, and then with the primary antibodies in antibody buffer (5% bovine serum albumin containing 0.3% Triton X-100 in PBS) at 4°C overnight. For each experiment, a pair of antibodies of different species was used. Next, cells were washed two times with buffer A for 5 min, followed by incubation with DuoLink PLA probes diluted in antibody diluent, in a pre-heated humidity chamber for one hour at 37°C. The following steps of ligation, amplification and washing were performed according to the manufacturer's protocol. Fluorescence was detected using Leica Stellaris 5 (Inverted) confocal.

RNA sequencing and ChIP-sequencing studies

Primary tumor xenografts harvested from the control and treatment groups were subjected to RNA-Seq. MDA-MB-231 cells treated with p38i, EPZ, combination or control were subjected to ChIP-Seq. RNA-Seq and ChIP-Seq were performed at the University of Michigan UMICH Advanced Genomics Core. Bioinformatics analysis was performed by the University of Michigan Bioinformatics Core using Advaita iPathwayguide https://ipathwayguide.advaitabio.com/dashboard.

QUANTIFICATION AND STATISTICAL ANALYSIS

Data are represented as mean ± SEM, and experiments were performed at least in triplicate. Differences between two groups were examined by Student's *t* test. We employed a non-parametric Mann-Whitney U test for the comparison of cell motility in microfluidics, as these data do not follow a normal distribution. To examine the gene ontology significances as pathway analyses, we employed Fisher exact test. In all statistical analyses, a p value of <0.05 was considered significant, with *$p \leq 0.05$; **$p \leq 0.01$; ***$p \leq 0.005$; ****$p \leq 0.0001$. The specific test used in each experiment can be found in the figure legends.